

# A novel method for wind farm layout optimization based on wind turbine selection

Giovanni Gualtieri

National Research Council, Institute of Biometeorology (CNR-IBIMET), Via Caproni 8, 50145 Firenze, Italy



## ARTICLE INFO

**Keywords:**

Wind farm layout optimization (WFLO)  
Wake model  
Wind turbine database  
Wind turbine spacing  
Levelized cost of energy (*LCoE*)  
Self-organizing map (SOM)

## ABSTRACT

A novel method was developed to detect the optimal onshore wind farm layout driven by the characteristics of all commercially-available wind turbines. A huge number of turbine combinations (577) was processed, resulting in 22,721 generated layouts. Various assumptions and constraints were considered, mostly derived from the literature, including site features, wind conditions, and layout design. For the latter, an irregularly staggered turbine array configuration was assumed. Wake effects were simulated through the Jensen's model, while a typical turbine thrust coefficient curve as a function of wind speed was originally developed. A detailed cost model was used, with levelized cost of energy selected as primary and capacity factor as secondary objective function. The self-organizing maps were used to address a thorough analysis, proving to be a powerful means to straightforwardly achieve a comprehensive pattern of wind farm layout optimization.

In general, the two optimization functions basically match, while for higher wind potential sites, increasing capacity factor did not necessarily result in decreasing levelized cost of energy. The latter may be minimised by reducing the total number of turbines or the overall wind farm capacity, as well as maximising rotor diameters or minimising rated wind speeds; increasing rated power or hub height is only beneficial for mid-potential sites. The mere maximisation of wind farm energy production is a misleading target, as corresponding to mid-to-high values of levelized cost of energy. In contrast to previous studies, the use of turbines with different rated power, rotor diameter or hub height should be avoided.

## 1. Introduction

In the last few decades, wind farm layout optimization (WFLO) has received great attention in wind energy studies. WFLO is generally intended as the optimum placement of wind turbines (WTs) in a wind farm (WF) aiming at minimizing energy losses due to the wake interference between them, thus maximizing the annual energy yield (AEY) [1]. However, since a WF planning is essentially an economical project, many Authors (e.g. [2]) claim that it is more meaningful to take minimisation of the cost of energy as primary objective function. Two schemes of WF layouts are generally considered when addressing the WFLO problem [3]: (i) array-based WF layouts, either placing WTs according to aligned or staggered arrays (e.g., [4]); (ii) grid-based WF layouts, i.e. layouts that divide the WF into a discrete grid (row/column-like) with WTs located over specific grid cells (e.g., [5]). Whatever the layout scheme, a common goal is pursued in achieving the best WTs positioning by detecting, respectively: (i) the optimal combination of crosswind and downwind distances between the WTs; (ii) the optimal cells of the grid where to place the WTs.

### 1.1. Motivation and background

WFLO is a multi-purpose (involves multiple objective functions) and a multi-variable (is influenced by a large number of variables) problem. Even for the simplest approach (i.e. AEY maximisation), it is a highly complex problem as, even for a low number of WTs (< 30), may lead to more than  $10^{44}$  potential solutions [6]. Furthermore, the WFLO is a non-convex problem since having many optimal solutions, so that optimization may converge to local rather than global optima [7]. Therefore, WFLO cannot be solved using traditional optimization methods, which led most authors to use meta-heuristic optimization techniques [8]. The latter include, e.g., Genetic Algorithms (GA) [9], Particle Swarm Optimization (PSO) [10], Random Search (RS) [11], or Ant Colony Optimization (ACO) [12]. Given the complexity of the WFLO problem, a number of assumptions and constraints shall necessarily be considered, which may involve site features, wind conditions, layout scheme (as described above), or WT characteristics.

As pointed out, e.g., by Castellani et al. [13], a further critical issue affecting the WFLO problem is given by the structural loading experienced by the WTs. As shown by various Authors (e.g., [14]), wake

E-mail address: [g.gualtieri@ibimet.cnr.it](mailto:g.gualtieri@ibimet.cnr.it).

## Nomenclature

### Abbreviations, notations and subscripts

|          |                               |
|----------|-------------------------------|
| AGL      | above ground level            |
| ANN      | artificial neural network     |
| ASL      | above sea level               |
| BL       | bottom-left                   |
| BR       | bottom-right                  |
| PL       | power law                     |
| SOM      | self-organizing map           |
| TL       | top-left                      |
| TR       | top-right                     |
| WF       | wind farm                     |
| WFLO     | wind farm layout optimization |
| WT       | wind turbine                  |
| <i>i</i> | upstream WT(s)                |
| <i>j</i> | downstream WT(s)              |
| w0.5, w1 | wind case studies (Fig. 3)    |
| <i>x</i> | prevailing wind direction     |
| <i>y</i> | crosswind direction           |

### Variables

|                      |  |
|----------------------|--|
| <i>a</i>             | WT axial induction factor [–], Eq. (2)   |
| <i>A</i>             | WT swept area [ $\text{m}^2$ ]   |
| $\alpha$             | wake expansion coefficient of upstream WT [–], Eq. (4)                                   |
| $\bar{\alpha}$       | wind shear coefficient [–]   |
| AEY                  | annual energy yield [MWh/y]  |
| $A_{overlap}$        | overlap area between upstream WT wake and downstream WT rotor [ $\text{m}^2$ ], Eq. (10) |
| $A_w$                | area of wake expansion caused by an upstream WT [ $\text{m}^2$ ]                         |
| CF                   | capacity factor [%]  |
| $C_i$                | annual cost at year <i>i</i> [\$/kW/y]   |
| $C_{ini}$            | initial capital cost [\$]  |
| $C_T$                | WT thrust coefficient [–]  |
| $D$                  | WT rotor diameter [m]  |
| $\delta$             | wind speed deficit [–], Eqs. (5), (13)   |
| $\Delta_x, \Delta_y$ | spacing between WTs along <i>x</i> and <i>y</i> directions [m]                           |
| $F_{site}$           | power losses of a single WT depending on the site type                                   |

|                 |   |
|-----------------|---|
| $F_{tot}$       | [%], Eq. (23)<br>total power losses of a single WT experienced in the WF                          |
| $F_{wake}$      | [%], Eq. (24)<br>power losses of a single WT due to all wake interactions in the WF [%], Eq. (19) |
| $F_{WT}$        | power losses of a single WT depending on the WT system [%], Eq. (22)                              |
| $\Phi$          | WT design ratio [–], Eq. (27)   |
| $H_{hub}$       | WT hub height [m]   |
| $\eta$          | WF efficiency [%], Eq. (21)   |
| $LCoE$          | levelized cost of energy [\$/MWh], Eq. (29)   |
| $L_x, L_y$      | size of WF along <i>x</i> and <i>y</i> directions [m]   |
| $N_P, N_D, N_H$ | number of combinations in the WF with WTs having different $P_r$ , $D$ or $H_{hub}$ [–]           |
| $N_T, N_{TH}$   | number of WTs, and number of “surrogated” WTs [–]   |
| $N_{WF}$        | number of WF layouts [–]  |
| $P$             | total wind power installed in the WF [kW]   |
| $P_e$           | electric power output from a WT [kW], Eq. (17)  |
| $P_m$           | mechanical power output from a WT [kW], Eq. (16)  |
| $P_r$           | WT rated power [kW]   |
| $R$             | WT rotor radius [m]   |
| $r_0$           | wake radius downstream a WT [m], Eq. (1)  |
| $r_w$           | radius of wake expansion caused by an upstream WT [m], Eq. (3)                                    |
| $\rho$          | air density [ $\text{kg}/\text{m}^3$ ]  |
| $s_x, s_y$      | multipliers of WT rotor diameters along <i>x</i> and <i>y</i> directions [–]                      |
| $v(z)$          | wind speed at generic height <i>z</i> AGL [m/s]   |
| $v, v_m$        | wind speed, and mean wind speed [m/s]   |
| $v_0$           | free stream wind speed [m/s]  |
| $v_{act}$       | actual wind speed approaching the WT [m/s], Eq. (14)  |
| $v_{hub}$       | actual wind speed approaching the WT at $H_{hub}$ [m/s]   |
| $v_b, v_r, v_o$ | WT cut-in, rated and cut-off wind speeds [m/s]  |
| $Z$             | height AGL [m]  |
| $z_0$           | aerodynamic surface roughness length [m]  |
| $z_{ref}$       | wind reference height AGL [m]   |
| $z_{site}$      | site elevation ASL [m]  |
| $\Omega$        | mean-to-rated wind speed [%], Eq. (28)  |

interactions between neighbour WTs may increase the fatigue damage on WTs, thus decreasing their expected lifetime within the WF. According to the review by Yuan and Tang [15], energy capture maximisation shall concurrently combine with structural load mitigation, and a proper balance between these two key aspects shall be pursued.

### 1.2. Literature survey

The first systematic approach for optimum placement of WTs in a WF was introduced by Mosetti et al. [16], who applied a GA algorithm to a gridded WF layout using Jensen's model [17] to calculate the wake effects between the WTs [1]. The objective function was concurrent maximisation of AEY and minimization of WTs installation costs [8]. The following assumptions and constraints were considered: (i) a flat onshore site; (ii) three theoretical wind scenarios; (iii) a single WT model installed all over the WF; (iv) a square gridded layout sized 2 km × 2 km with square cells each sized 200 m (i.e. 5 rotor diameters) being possible location of a WT [16]. Since this pioneering work, a huge number of WFLO studies were carried out, focussing on either gridded or array-based layouts: however, to date (e.g., [18] for gridded and [19] for array layouts), in the vast majority of such studies best WT allocation was the solely pursued WFLO target. Conversely, as pointed out by Chowdhury et al. [20], the WFLO problem should pursue two key

aspects that are necessarily part of a synergistic goal: (i) best WTs allocation, and (ii) best WTs selection. While a very huge body of literature exists on the above-mentioned optimization algorithms – actually used as mere “best allocators”–, few studies focused on detecting the most suitable physical and operational characteristics of commercial-scale WTs, thus treating WTs within the WF as living entities rather than mere “pawns to be moved on a chessboard”. Actually, there are so many WT parameters (e.g. rotor diameter, hub height, cut-in and rated wind speed, rated power, type of generator or gearbox, etc.) that increase the practical difficulty of optimization [2]. The benefits of using multiple types of WTs installed in a particular WF arrangement were rarely explored in the literature [20]. And, even when this was addressed, to the best of the Author's knowledge, a maximum of 61 WTs [21] were used so far. To summarize, WT characteristics cannot be considered an additional problem assumption, but rather a portfolio of variables to be careful analysed in order to detect the unique combination that really satisfies the WFLO problem. This specific issue was clearly urged by various Authors (e.g., [4]) as a future WFLO research direction.

Thrust coefficient  $C_T$  is one of the design characteristics of a WT rotor [3], playing a major role in the WF wake analysis. Unfortunately, in the vast majority of WFLO studies (e.g. [22]), a fixed 0.88 value is assumed, which is not accurate if analysing the available  $C_T$  curves for

commercial WTs. According to Abdulrahman and Wood [21], to develop realistic  $C_T$  patterns for commercial WTs is one of main deficiencies reviewed in the past WFLO literature. To this aim, they developed a  $C_T$  continuous curve as a function of power coefficient  $C_p$ . On the other hand, very few WFLO studies (e.g. [23]) treated  $C_T$  as a variable value depending on wind speed in accordance with the experimental curves supplied by WT manufacturers. Ali et al. [24], for example, proposed for  $C_T$  a theoretical evolution with wind speed.

### 1.3. Contribution of the paper

The major contributions of this paper are the following:

- a novel WFLO method is proposed based on the characteristics of all WTs effectively available in the market, thus mainly focussing on WT selection rather than on mere WT best allocation, often performed disregarding the WT characteristics;
- a huge number (200) of onshore commercial WTs is used, the highest among all WFLO studies carried out in the literature;
- based on commercial WT data, an empirical equation is originally developed to derive a typical  $C_T$  curve as a function of wind speed, thus avoiding the use of a constant  $C_T$  value;
- the highly complex, non-convex, multi-variable and multi-purpose nature of the WFLO problem requires the use of advanced rather than traditional analysis tools: to this aim, the self-organizing map (SOM), a type of unsupervised learning ANN-based model, is used.

The method was developed for an onshore and sea-level site with

flat terrain, focussing on a  $2\text{ km} \times 2\text{ km}$  square WF layout. Two different wind scenarios with multiple direction and intensity have been considered. Both these site- and wind-related assumptions have been derived from the WFLO literature [16]. Again based on literature findings, an array of unequally spaced WTs was considered. According to Wang et al. [25], for example, when compared to the discrete grid-based WF design method, the continuous coordinate method has the property of continuously varying the placement of WTs, and hence, it is more capable of obtaining the global optimum solutions. Wake effects were simulated through the Jensen's model. A detailed cost model was used, with leveled cost of energy (LCoE) selected as primary and capacity factor (CF) as secondary WFLO objective function.

The remainder of the paper is organized as follows. In Section 2, the wake model, the analytic method to calculate all losses other than wake losses, the developed  $C_T$  curve, the cost model, and the SOMs are presented. WFLO assumptions and constraints are described in Section 3. The developed WFLO procedure is detailed in Section 4. Section 5 provides a full discussion on the achieved results, particularly on the detected optimal WF layouts and – thanks to the SOMs – on main issues lying behind.

## 2. Methods

The present WFLO has been addressed by using Jensen's model to calculate wake losses between the WTs, an analytic method to assess all other losses in the WF, an originally-developed  $C_T$  curve as a function of wind speed, and the NREL cost model. The SOMs were used to perform an advanced analysis of the WFLO achieved results.

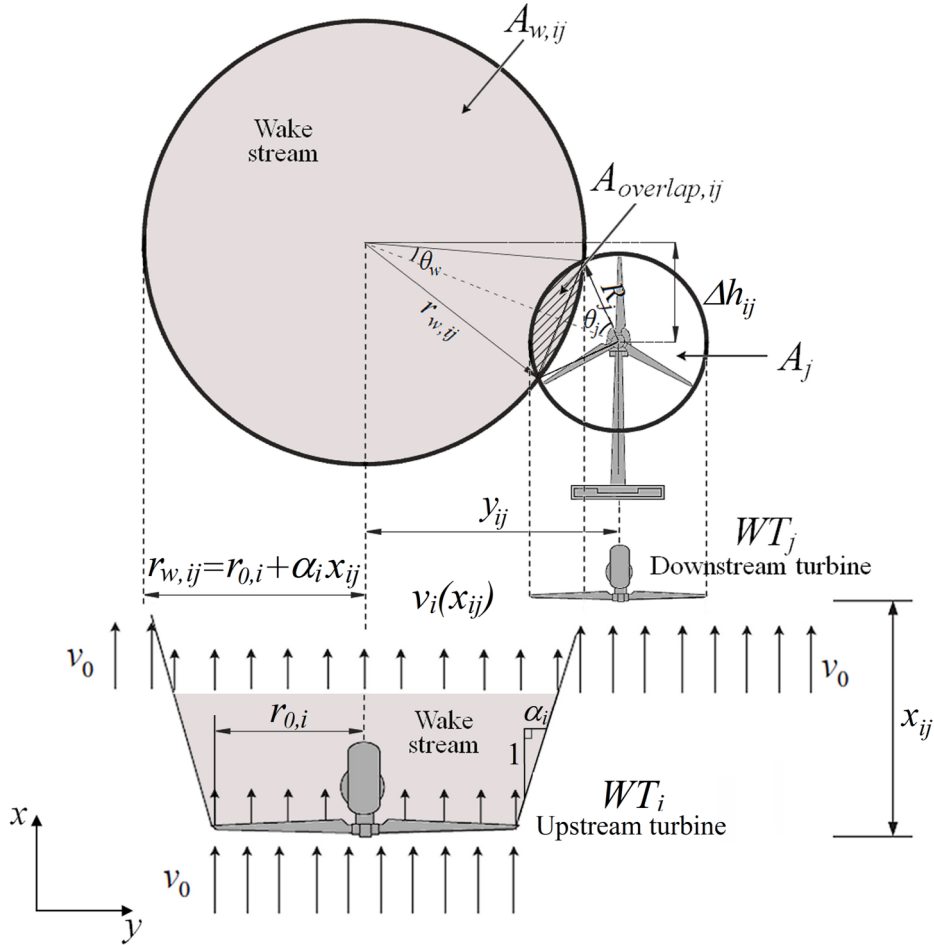


Fig. 1. Schematic of Jensen's wake model and partial shadowing caused by the wake effect induced by upstream  $WT_i$  on downstream  $WT_j$  (adapted from Refs. [27;31]).

## 2.1. Wake effect: Jensen's wake model

Downstream WTs in a WF undergo a decreased wind energy because of the wake effect caused by the upstream WTs [26]. Wake interactions among WTs are quantitatively assessed by applying the wake models [27]. Among many wake models developed over the last few decades, analytical wake models, based on similar velocity deficit profiles, are generally the most straightforward [27]. Jensen's analytical wake model is one of the simplest and most accurate in calculating both velocity and power deficits within a WF [21]. Originally proposed by Jensen [17], this model was later tuned to study the WFLO [28], which is known as the PARK model. It was implemented in the majority of WFLO studies and in most WFLO software packages [21], such as WAsP [29] and WindPro [30].

Jensen's model assumes a linear expansion of the wake behind a WT and a constant wind speed deficit in the radial direction [27] (Fig. 1). If assuming a uniform free wind speed  $v_0$  blowing along the  $x$  direction, the radius of the wake spreading downstream  $WT_i$  is given by [27]:

$$r_{0,i} = R_i \sqrt{\frac{1 - a_i}{1 - 2a_i}} \quad (1)$$

where  $R_i$  is  $WT_i$  rotor radius and  $a_i$  its axial induction factor, defined as [31]:

$$a_i = 0.5(1 - \sqrt{1 - C_{T,i}}) \quad (2)$$

with  $C_{T,i}$  the  $WT_i$  thrust coefficient.

The radius of wake expansion caused by  $WT_i$  at radial distance  $x_{ij}$  of downstream  $WT_j$  is [27]:

$$r_{w,ij} = r_{0,i} + \alpha_i x_{ij} \quad (3)$$

where  $\alpha_i$  is the wake expansion coefficient of  $WT_i$ , given by the empirical equation [31]:

$$\alpha_i = \frac{0.5}{\ln(H_{hub,i}/z_0)} \quad (4)$$

with  $H_{hub,i}$  the  $WT_i$  hub height and  $z_0$  site's aerodynamic surface roughness length.

According to the momentum theory, for a single wake between two WTs, the velocity deficit denoting the wind speed reduction from free air stream to the air in the wake is [32]:

$$\delta_{ij} = 2a_i \left( \frac{r_{0,i}}{r_{w,ij}} \right)^2 \sqrt{\frac{A_{overlap,ij}}{A_j}} \quad (5)$$

where  $A_j$  is  $WT_j$  swept area, and  $A_{overlap,ij}$  is the overlap area between  $A_j$  and the upstream  $WT_i$  wake area at  $x_{ij}$  ( $A_{w,ij}$ ) (Fig. 1).

The method reported, e.g., by Ref. [27] can be used to calculate the overlap area  $A_{overlap,ij}$  in Eq. (5) between the area of wake expansion caused by the upstream  $WT_i$  at  $x_{ij}$  ( $A_{w,ij}$ ) and the downstream  $WT_j$  rotor area ( $A_j$ ), and thus their wake interaction (Fig. 1). Thus, the following distances are introduced:

$$D_{dot} = x_{ij} \cos(\theta) + y_{ij} \sin(\theta) \quad (6)$$

$$D_{cross} = x_{ij} \sin(\theta) - y_{ij} \cos(\theta) \quad (7)$$

where  $x_{ij}$  and  $y_{ij}$  are the along-wind and crosswind distances between  $WT_i$  and  $WT_j$ , respectively, and  $\theta$  is the wind direction.

If denoting  $\Delta h_{ij}$  as the difference between hub heights of  $WT_i$  and  $WT_j$ , and  $R_j$  the downstream  $WT_j$  rotor radius, a partial wake occurs when both the following conditions apply:

$$\begin{cases} D_{dot} > 0 \\ r_{w,ij} - R_j < \sqrt{|D_{cross}|^2 + \Delta h_{ij}^2} \leq r_{w,ij} + R_j \end{cases} \quad (8)$$

A full wake occurs when both the following conditions apply:

$$\begin{cases} D_{dot} > 0 \\ \sqrt{|D_{cross}|^2 + \Delta h_{ij}^2} \leq r_{w,ij} - R_j \end{cases} \quad (9)$$

When neither conditions defined in Eqs. (8) and (9) are satisfied, no wake occurs between the two WTs.

For no wake pattern,  $A_{overlap,ij}$  is equal to zero, and so is  $\delta_{ij}$  in Eq. (5). For the full wake,  $A_{overlap,ij}$  is equal to  $A_j$  [27]. For the partial wake case,  $A_{overlap,ij}$  can be calculated through arithmetical operations based on the relationship between WTs positions [27]:

$$A_{overlap,ij} = r_{w,ij}^2 [\theta_w - \sin(2\theta_w)/2] + R_j^2 [\theta_j - \sin(2\theta_j)/2] \quad (10)$$

where:

$$\theta_w = \arccos[(r_{w,ij}^2 + x_{ij}^2 + \Delta h_{ij}^2 - R_j^2)/(2r_{w,ij}\sqrt{x_{ij}^2 + \Delta h_{ij}^2})] \quad (11)$$

$$\theta_j = \arccos[(R_j^2 + x_{ij}^2 + \Delta h_{ij}^2 - r_{w,ij}^2)/(2R_j\sqrt{x_{ij}^2 + \Delta h_{ij}^2})] \quad (12)$$

Summarizing, for a  $WT_j$  affected by multiple wakes caused by up to  $N_i$  upstream  $WT_i$ , the overall velocity deficit can be calculated by summing up the  $N_i$  contributions given by Eq. (5) [32]:

$$\delta_j = \sqrt{\sum_{i=1}^{N_i} \delta_{ij}^2} = \sqrt{\sum_{i=1}^{N_i} \left[ 2a_i \left( \frac{r_{0,i}}{r_{w,ij}} \right)^2 \sqrt{\frac{A_{overlap,ij}}{A_j}} \right]^2} \quad (13)$$

Therefore, actual wind speed approaching the downstream  $WT_j$  can be expressed as:

$$v_{act,j} = v_0(1 - \delta_j) \quad (14)$$

## 2.2. Wind farm efficiency and total power losses

If considering a WT with swept area  $A$  affected by a given wind speed  $v$ , site's available wind power is [33]:

$$P(v) = \frac{1}{2} \rho A v^3 \quad (15)$$

where  $\rho$  is the air density.

The mechanical power  $P_m(v)$  that can be extracted from site's available wind power is [34]:

$$P_m(v) = C_p P(v) = \frac{1}{2} C_p \rho A v^3 \quad (16)$$

where  $C_p$  is WT power coefficient, whose theoretical maximum value (0.593) is the Betz limit.

The electric power output  $P_e(v)$  from a real WT is given by Ref. [35]:

$$P_e(v) = \eta_m \eta_e P_m(v) = \frac{1}{2} C_p \eta_m \eta_e \rho A v^3 = \frac{1}{2} \eta_T \rho A v^3 \quad (17)$$

where  $\eta_m$  and  $\eta_e$  are the efficiencies of mechanical transmission and electric generation, and  $\eta_T = C_p \eta_m \eta_e$  is the WT total power efficiency [35].

If assuming a standard value for  $\rho$  (1.225 kg/m<sup>3</sup>), a 40% for  $\eta_T$ , and a WT rotor radius of 20 m, manipulation of Eq. (17) as shown, e.g., by Rajper and Amin [33], yields:

$$P_e(v) = 0.3 v^3 \quad (18)$$

with  $P_e(v)$  in kW.

Combining Eqs. (14) and (18), the total power losses of  $WT_j$  due to all wake interactions affecting the WT in the farm can be calculated as:

$$F_{wake,j} = 1 - \frac{P_{act,j}}{P_0} = 1 - \frac{v_{act,j}^3}{v_0^3} \quad (19)$$

with  $P_{act,j}$  and  $P_0$  the power productions related to  $v_{act,j}$  and  $v_0$ , respectively.

Efficiency is a metric quantifying the amount of energy extracted as apart of the total energy available [33]. In general, WF efficiency is defined as the ratio between total actual power production and total

ideal power production [23]:

$$\eta = P_{act}/P_{ideal} \quad (20)$$

Therefore, if considering a WF comprising  $N$  WTs, WF efficiency can be calculated by combining Eqs. (18) and (20) [33]:

$$\eta = \frac{\sum_{j=1}^N P_{act,j}}{N P_0} = \frac{\sum_{j=1}^N 0.3 v_{act,j}^3}{N (0.3 v_0^3)} \quad (21)$$

where  $v_{act,j}$  is the actual wind speed approaching any generic WT<sub>j</sub> (Eq. (14)). Eq. (21) is consistent with Mosetti et al. [16], who defined  $\eta$  as the ratio between the total energy extracted by a WF comprising  $N$  WTs and  $N$  times the energy extracted by an isolated WT affected by the same undisturbed wind.

Total power losses for a single WT – excluding wake losses (Eq. (19)) – can be calculated through the analytical method described in Ref.

[36] as a combination of: (i) WT-specific losses (for gearbox, generator, converter, and unavailability & repair); (ii) site-specific losses (for electric grid connection, icing/soiling, and other).

WT-specific losses  $F_{WT}$  are given by:

$$F_{WT} = 1 - [(1 - f_{gearbox})(1 - f_{generator})(1 - f_{converter})(1 - f_{unav})] \quad (22)$$

while site-specific losses  $F_{site}$  are given by:

$$F_{site} = 1 - [(1 - f_{grid})(1 - f_{ice})(1 - f_{other})] \quad (23)$$

The above values of  $f_x$  factors for each single loss are detailed as a function of WT system and site type in Table 3 of [36]. Note that, since through Eq. (22) WT different system types are taken into account, this method provides a further WT distinction by WT characteristics.

Therefore, total power losses for a single WT<sub>j</sub>  $F_{tot,j}$  – including wake losses (Eq. (19)) – are:

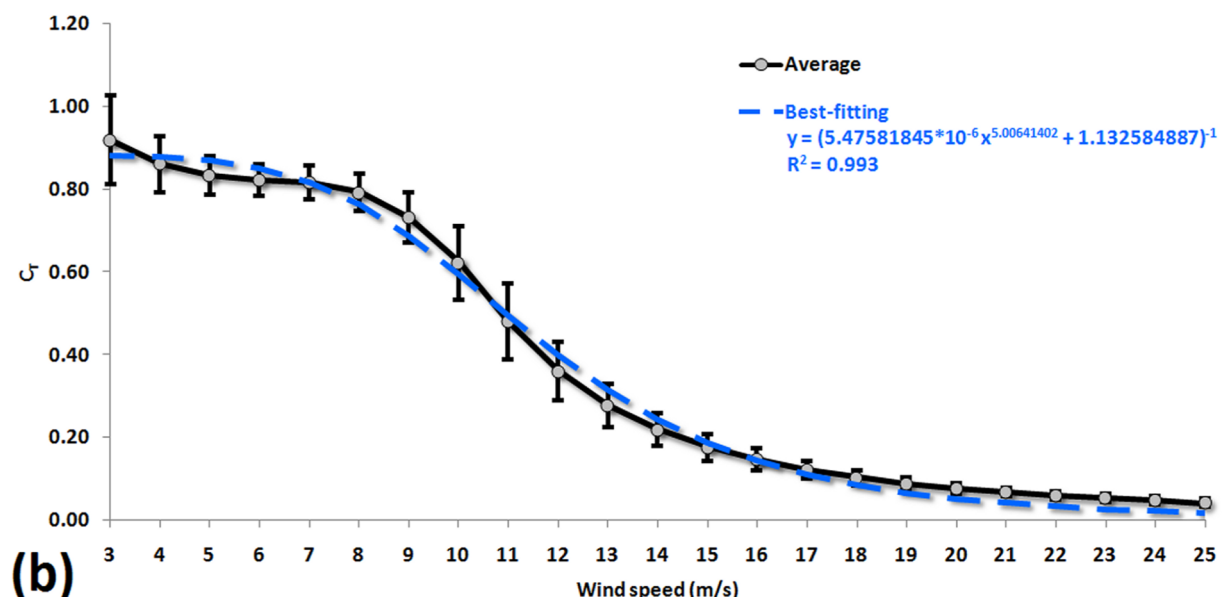
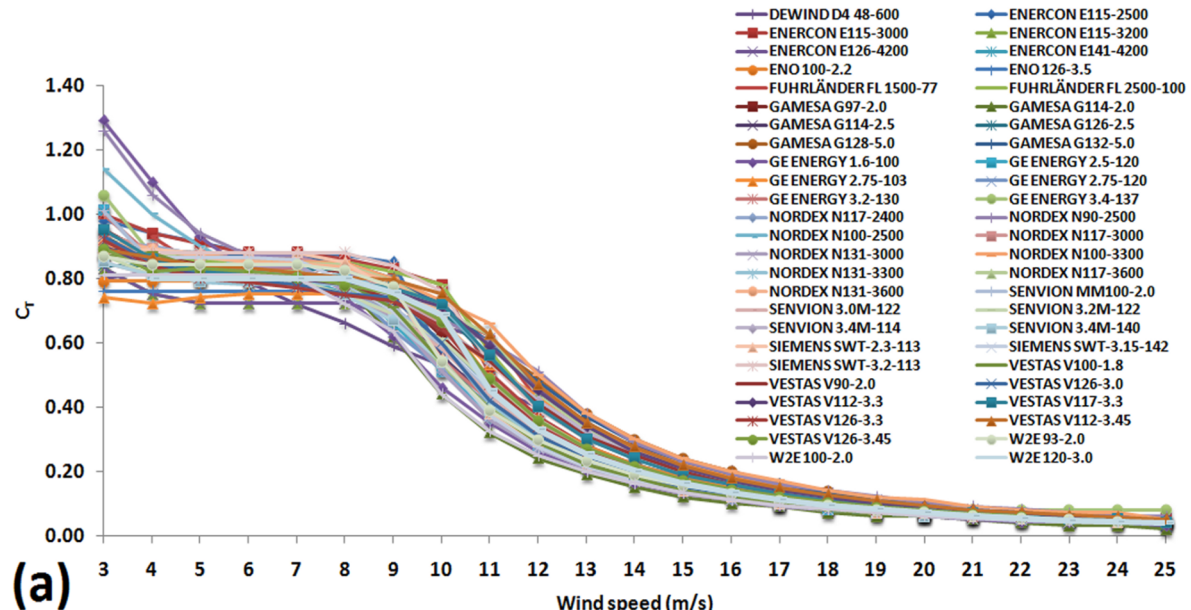


Fig. 2. Thrust coefficient curves as a function of wind speed: (a) real data retrieved from 50 commercial WTs [37]; (b) average and best-fitting curves.

$$F_{tot,j} = 1 - [(1 - F_{WTj})(1 - F_{site})(1 - F_{wake,j})] \quad (24)$$

### 2.3. Wind turbine thrust coefficient and derived parameters

As shown in Eq. (2),  $C_T$  is a crucial WT parameter to assess an accurate wake analysis. To overcome the common approximation of using the  $C_T = 0.88$  constant value, based on  $C_T$  data available from 13 commercial WTs, Abdulrahman and Wood [21] developed a  $C_T$  continuous curve as a function of  $C_p$  in the form of a 5th degree polynomial best-fitting (see Fig. 3 therein).

For a WT, the  $C_T$  curve is usually provided by manufacturers as a function of the free wind speed  $v_0$  [27]. However, as reviewed by Serrano et al. [8], in WFLO studies  $C_T$  was rarely considered as a value varying with wind speed. Ali et al. [24], for example, proposed the following theoretical formulation:

$$C_T = 3.5(2v - 3.5)/v^2 \approx 7/v \quad (25)$$

A further improvement is proposed herein. Based on  $C_T$  real data available from 50 commercial WTs [37] (Fig. 2a), an average curve and a best-fitting curve have been calculated (Fig. 2b), with the latter resulting in the form:

$$C_T = (5.47581845 * 10^{-6}v^{5.00641402} + 1.132584887)^{-1} \quad (26)$$

which returned  $R^2 = 0.993$ . The explicit values of average, standard deviation and best-fitting  $C_T$  values as a function of binned wind speeds are tabulated in Table S1 of the Supplementary material.

Additional parameters – derived as a combination of basic parameters – may be introduced to better assess WT characteristics.

The WT design ratio, for example [35]:

$$\Phi = v_r/v_i \quad (27)$$

is a crucial WT regulation parameter since returning the range of the  $v_i$ – $v_r$  operating region:  $\Phi$  influence played on WT site optimization was extensively analysed in [35].

A further parameter, allowing to assess WT performances once paired with site's characteristics, may be introduced as ratio between site's mean wind speed and WT rated wind speed:

$$\Omega = v_m/v_r \quad (28)$$

This mean-to-rated wind speed  $\Omega$  allows to quantify the fraction of wind speed that the WT is capable of satisfying when working at rated conditions. When considering a real WF,  $v_m$  in Eq. (28) should be intended as the  $v_m$  actually approaching the WT at its  $H_{hub}$ , i.e.  $v_{act}$  (Eq. (14)) with  $z = H_{hub}$ . Overall,  $\Omega$  can be thought of as the equivalent to wind speed of  $CF$  to energy yield.

### 2.4. Wind turbine cost estimation

The leveled cost of energy ( $LCoE$ ) is the metric most commonly used to assess the economic viability of a WF project [34]. It is defined as the ratio between lifetime costs and lifetime electricity generation, both discounted back to a common year through a discount rate that reflects the average capital cost [38].  $LCoE$  for a WF project is calculated as [36]:

$$LCoE = \frac{C_{ini} + \sum_{i=1}^n C_i/(1+d)^i}{\sum_{i=1}^n AEY/(1+d)^i} \quad (29)$$

where  $C_{ini}$  is the initial capital cost,  $C_i$  the annual cost at year  $i$  since installation,  $n$  the operational life [years], and  $d$  [%] the interest rate of the investment. The initial capital cost  $C_{ini}$  of a WF project is the sum of the WT capital cost, the balance of system, and financial costs. Annual costs  $C_i$  include operation and maintenance costs.

As pointed out by Wang et al. [32], WFLO results strongly depend on the selected WF cost model, which is therefore a crucial component of the whole process. Various empirical cost models have been

proposed in the literature, such as the very simplified one proposed by Mosetti et al. [16], which relates the WF cost to the number of installed WTs through a single equation. A more refined model was proposed by Chen et al. [39], which also takes  $P_r$  into account. The most thorough cost model is probably the analytical model developed at NREL by Fingersh et al. [40], which details the cost of each single WT component and subsystem. Details of this model are fully reported in Ref. [2], where: (i)  $C_{ini}$  is given in Table 1 as a function of  $R$ ,  $P_r$  and  $H_{hub}$  by means of 23 equations; (ii)  $C_i$  is given in Table 2 as a function of  $P_r$  and

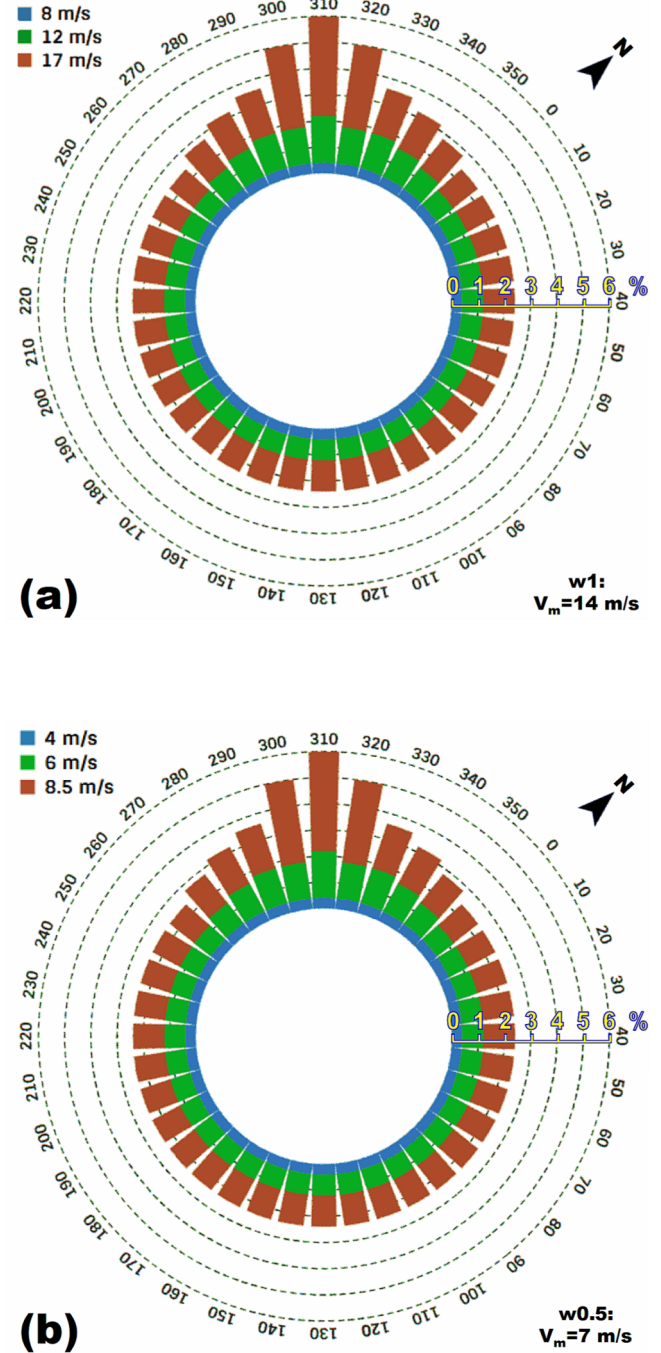


Fig. 3. Polar representation with occurrence distribution (%) of the assumed wind conditions: (a) multi-directional wind with variable intensity ( $w1$ ) [16]; (b) same as (a), but with halved wind magnitudes ( $w0.5$ ). For representation convenience, wind directions are rotated clockwise by  $50^\circ$  as such that prevailing wind directions are vertical. Overall mean wind speeds  $v_m$  are also reported.

**Table 1**

Assumptions and constraints for wind farm layout.

| Section  | Description | Parameter                  | Value(s)  |
|--|-------------|----------------------------|---|
| Site   |             |                            |   |
| Location   |             |                            | onshore   |
| Topography   |             |                            | flat  |
| Elevation  |             | $z_{site}$                 | 0 m ASL   |
| Aerodynamic surface roughness length                   |             | $z_0$                      | 0.30 m  |
| Wind shear coefficient                                 |             | $\alpha$                   | 0.20  |
| Air density  |             | $\rho$                     | 1.225 kg/m <sup>3</sup>   |
| Wind conditions  |             |                            |   |
| Wind case studies                                      |             | $w1$                       | multi-directional wind with variable wind speed ( $v_m = 14$ m/s, Fig. 3a)  |
|  |             | $w0.5$                     | same as $w1$ , but with halved wind speeds ( $v_m = 7$ m/s, Fig. 3b)  |
| Reference height                                       |             | $z_{ref}$                  | 60 m AGL  |
| Vertical profile                                       |             | $v(z)$                     | varying based on PL   |
| Wind turbines  |             |                            |   |
| No. Models   |             | $N_T$                      | 200   |
| No. “surrogated” WT models, i.e. sorted by hub heights |             | $N_{TH}$                   | 577   |
| Thrust coefficient                                     |             | $C_T$                      | varying with wind speed (Eq. (26), Fig. 2b)   |
| Power curve  |             |                            | WT-specific, i.e. not approximated  |
| WF layout design criteria (Fig. 4)                     |             |                            |   |
| Layout size  |             |                            |   |
| downwind (x)   |             | $L_x$                      | 2000 m  |
| crosswind (y)  |             | $L_y$                      | 2000 m  |
| WT placement   |             |                            | Irregularly staggered array configuration: WTs aligned and equally spaced along the crosswind direction, while staggered and unequally spaced along the prevailing wind direction |
| WT spacing <sup>a</sup>                                |             |                            |   |
| downwind (x)   |             | $\Delta_x = s_x * D_{i-1}$ | $s_x$ rotor diameters of the upwind row WTs   |
| crosswind (y)  |             | $\Delta_y = s_y * D_i$     | $s_y$ rotor diameters of the same row WTs   |
| WT selection criteria                                  |             |                            |   |
| manufacturer(s)  |             |                            | The same for the whole WF   |
| WT model(s)  |             |                            | The same along the crosswind direction, and varied along the downwind direction   |

<sup>a</sup> After the analysis in Section 5.1, the following WT spacing was set:  $s_x = s_y = 10$ .

**Table 2**Summary of characteristics of all processed onshore WTs.<sup>a</sup>

| Score        | Rated power | Rotor diameter | Hub height | Wind speeds           |                      |                        | Design ratio |
|--------------|-------------|----------------|------------|-----------------------|----------------------|------------------------|--------------|
|              |             |                |            | Cut-in<br>$v_i$ (m/s) | Rated<br>$v_r$ (m/s) | Cut-off<br>$v_o$ (m/s) |              |
| Median value | 2000        | 82             | 80         | 3.0                   | 13.0                 | 25.0                   | 4.0          |
| Range        | 500–7580    | 39–152         | 35–164     | 2.0–5.0               | 10.0–18.0            | 20.0–28.0              | 2.8–7.5      |

<sup>a</sup> Total WT models:  $N_T = 200$ . Total “surrogated” WT models, i.e. sorted by  $H_{hub}$ :  $N_{TH} = 577$ .

AEY based on 3 equations. Such NREL cost model was applied in the present work, where cost parameters have been estimated taking the 2019 US market as a reference and [+] as currency. In addition, since the NREL cost model was developed based on a 2002 survey, an inflation scaling factor (equal to 1.34) accounting for the US average inflation rate between 2002 and 2019 has been considered to update both  $C_{ini}$  and  $C_i$ .

## 2.5. Self-organizing map

Kohonen’s SOMs [41] have been successfully applied in various scientific disciplines to untangle complex patterns and detect hidden structures in high-dimensional datasets. In wind energy, for example, SOMs have been applied in wind speed spatial interpolation [42], WT fault diagnosis [43], and WT optimal site matching [36]. The SOM is an unsupervised learning ANN-based model implementing a nonlinear projection from a high-dimensional data space to a low-dimensional (usually 2-D) regular grid of neurons [41]. Mapping from the original data space (input layer) to the grid of neurons (output layer) is performed while preserving the most important topological and metric relationships of the primary data. The algorithm recognizes groups of similar input variables and organizes the neurons with similar feature

values close to each other on the map, while dissimilar data records are positioned on different map edges. The grid of neurons therefore allows to easily exploring the relationships between the variables and the possible cluster structure of the data [41].

## 3. Assumptions and constraints

Assumptions and constraints considered in the current WFLO procedure (Table 1) are mostly taken from the past literature in order to make WFLO results comparable.

### 3.1. Site features and wind conditions

Similarly to various WFLO studies in the literature (e.g. [16]), it has been assumed that the WF site is onshore, completely flat, at sea level ( $\rho = 1.225$  kg/m<sup>3</sup>), and with  $z_0 = 0.3$  m.

In addressing the WFLO problem, several Authors (e.g. [26]) relied upon an observed joint distribution of wind speed and direction. This approach has the advantage of actually adhering to the real world, yet – since too tailored to the specific case study – also the disadvantage of not allowing to generalise the WFLO outcomes. To this aim, it is therefore preferable to deal with pre-fixed wind conditions. Among the

**Table 3**  
Results of wind farm layout optimization by wind case study and optimization condition.<sup>a</sup>

| Optimization condition | WF layout | Wind case study | Cumulated |        |       | Mean                 |                      |                                    | Cumulated                          |       |  | Mean                      |             |        | Cumulated |               |
|------------------------|-----------|-----------------|-----------|--------|-------|----------------------|----------------------|------------------------------------|------------------------------------|-------|--|---------------------------|-------------|--------|-----------|---------------|
|                        |           |                 | No WTs    | P (kW) | D (m) | H <sub>hub</sub> (m) | v <sub>r</sub> (m/s) | Φ = v <sub>r</sub> /v <sub>t</sub> | Ω = v <sub>m</sub> /v <sub>t</sub> | H (%) | C <sub>inf</sub> /P <sub>r</sub> (\$/kW) | C <sub>i</sub> (\$/kWh/y) | AEY (MWh/y) | CF (%) | CF (%)    | LCoE (\$/MWh) |
| Maximising CF          | L1        | w0.5            | 4         | 8000   | 116   | 140                  | 10                   | 2.90                               | 71.10                              | 100   | 2309                                     | 465                       | 32,390      | 46.22  | 143.47    |               |
|                        | L2        | w1              | 4         | 8000   | 104.5 | 100                  | 11.25                | 3.25                               | 127.98                             | 100   | 1823                                     | 814                       | 64,595      | 92.17  | 112.11    |               |
| Minimising LCoE        | L3        | w0.5            | 9         | 7200   | 76.7  | 80                   | 11                   | 3.70                               | 59.61                              | 98.22 | 1996                                     | 345                       | 22,327      | 35.40  | 143.44    |               |
|                        | L4        | w1              | 9         | 7200   | 76.7  | 61.5                 | 11                   | 3.70                               | 120.35                             | 99.56 | 1878                                     | 706                       | 55,645      | 88.23  | 103.46    |               |

<sup>a</sup> Optimizations pursued over a total of 22,721 layouts built-up as in Fig. 4 with 10D × 10D WT spacing.

classical three wind case studies firstly introduced by Mosetti et al. [16] to define the free stream wind regime for WFLO computations, the most general one has been assumed herein, i.e. the one with variable intensity and direction (case ‘c’). Examples of use of this pre-fixed joint wind distribution may be found, e.g., in Ref. [22]. Fig. 3a gives a polar representation of this wind case study (termed “w1”), affected by three wind intensity (8, 12 and 17 m/s) and 36 wind directions – binned by 10°–, with unequal probability of occurrence by both intensity and direction. Wind occurrences are greater between 280 and 360°, with prevailing wind direction oriented by 310° from North: the 280–360° directions have therefore more effects on WF layout than other directions [39]. Again similarly to Mosetti et al. [16], reference wind blowing height ( $z_{ref}$ ) is 60 m AGL. Overall mean wind speed ( $v_m$ ) for wind condition w1 is 14 m/s, which corresponds, if applying the PL with  $\bar{\alpha} = 0.20$ , to a 60-to-50 m downscaled value of 13.50 m/s. Based on the NREL wind power classification [44], a site affected by  $v_m = 13.50$  m/s at 50 m has even more potential than a “superb” site, as its  $v_m$  is even higher than the upper limit (11.1 m/s) set for defining the top rank (7) wind power class. In order to also deal with a more realistic wind potential site, a further wind condition has been considered, featuring the same occurrence distribution of w1, yet with all wind magnitudes halved (Fig. 3b). This new wind condition (termed “w0.5”) has an overall  $v_m$  of 7 m/s at 60 m, corresponding to 6.75 m/s at 50 m. This is certainly a more realistic site, as falling into the 6.4–7.0 m/s wind speed range typical of a “fair” site [44], i.e. ranked 3 (out of 7).

In order to adjust reference wind conditions at  $z_{ref} = 60$  m to the varying magnitudes blowing at the specific WT  $H_{hub}$ , the PL has been used. Since the simplest and the most accurate wind speed extrapolation model, the PL is the most commonly used in the majority of wind energy applications (73.5%) [45]. To apply the PL, the value of wind shear coefficient  $\bar{\alpha}$  is required, which depends on several parameters including wind speed, atmospheric stability, terrain roughness, and the height interval [46]. When no site’s measurements or estimates are available for  $\bar{\alpha}$ , an average value as a function of landscape type can be used. Based on the look-up Table 1 reported in [47], for the selected site it was assumed  $\bar{\alpha} = 0.20$ . Notably, the PL was used to reproduce the wind speed profile across a “typical” atmospheric boundary layer, which is a rough simplification due to the turbulent nature of the wind. Over complex terrains, for example, local effects as hilltop speed-ups and lee-side deceleration and flow separation may result in wind profiles that the PL fails to reproduce [45]. On open-sea locations, the frequent development of internal boundary layers results in anomalous vertical profiles due to wind speed inflections at intermediate heights, which make the PL no longer applicable [45].

### 3.2. Wind turbines

A comprehensive WT database, implemented within the wind resource assessment tool described in Ref. [48] and later updated, has been used. The database includes more than 350 onshore commercial-scale models. Where unavailable from manufacturers’ official websites, WT characteristics have been retrieved from the WindPower database [49]. This WT database was also used to address the WT optimal site matching described in Ref. [36].

A total of  $N_T = 200$  onshore commercial WTs retrieved from the WT database has been used. This sub-sample was obtained by setting a minimum  $P_r = 500$  kW in order to filter out the lower-sized models. Overall, WTs are retrieved from 25 different manufacturers, with Vestas (21) and Nordex (16) delivering the highest number of models. A summary of main WT characteristics is provided by the histograms plotted in Fig. S1 of the Supplementary material, while Table 2 reports the corresponding median values and ranges. In particular,  $P_r$  ranges between 500 and 7580 kW,  $D$  between 39 and 152 m,  $H_{hub}$  between 35 and 164 m, and  $v_r$  between 10 and 18 m/s. Importantly, instead of being possibly fitted by means of polynomial, exponential, cubic or quadratic expressions (such as, e.g., in Ref. [2]), the experimental power curves

have been used for each WT.

WTs having multiple hub heights have been treated as distinct (or “surrogated”) WTs with respect to the basic model: thus, the total number of WT combinations summed up to  $N_{TH} = 577$ , which was *de facto* the number of WTs used in building-up any WF layout.

As for WT thrust coefficient, the  $C_T$  curve as a function of wind speed (Eq. (26)) was used.

Reliability of the NREL cost model has been roughly assessed after comparison with some literature studies. For example, for WTs with  $P_r$  between 1.8 and 2.0 MW an average  $C_{WT}/P_r$  of 1380 \$/kW was achieved, which is slightly higher than 1185 \$/kW reported by Moné et al. [50] for 2013-updated US land-based projects employing 1.91-MW WTs. A further thorough comparison, addressed against market prices, returned  $C_{WT}$  estimates well approximating the costs reported for some models by Boudia and Guerri [51]: 930 k\$ for Nordex N50-800 (vs. 970 k\$); 1260 k\$ for Neg-Micon 60-1000 (vs. 1315 k\$); 1820 k\$ for Vestas V66-1.65 (vs. 2000 k\$), and 3620 k\$ for Vestas V90-3.0 (vs. 3600 k\$).

### 3.3. Wind farm layout

Similarly to the past WFLO studies (e.g. [16]), a square WF layout sized ( $L_x \times L_y$ ) 2 km  $\times$  2 km was assumed. As depicted in Fig. 4, WTs are oriented downstream the prevailing wind direction  $x$ , which is rotated clockwise by 50° for representation convenience. Following findings from various studies (e.g., [52]), a staggered WT array configuration is assumed: WTs are aligned by row (i.e. along the crosswind direction  $y$ ), and staggered by column (i.e. along the downwind direction  $x$ ). WTs are regularly spaced along  $y$  (same  $\Delta_y$ ), while irregularly spaced along  $x$  (different  $\Delta_x$ ). For any layout instance, a “realistic” criterion is followed in choosing a common manufacturer for all WTs installed in the WF. WTs are extracted from the WT database and all their possible combinations deriving from varying model,  $D$  and  $H_{hub}$  are implemented. WTs are the same for each row (i.e. along  $y$ ), while they are varied from one row to the other (i.e. along  $x$ ). For a given row  $i$ , WTs are crosswind spaced as a function of their rotor diameter  $D_i$  through the crosswind multiplier  $s_y$  ( $\Delta_y = s_y * D_i$ ), while they are downwind spaced as a function of rotor diameter  $D_{i-1}$  of upwind row ( $i-1$ ) WTs through the downwind multiplier  $s_x$  ( $\Delta_x = s_x * D_{i-1}$ ). WTs are laterally staggered by placing the first WT of the even rows at ( $1/2 * s_y * D_{i-1}$ ) from left-hand side boundary of the WF. Furthermore, since in general WT rotor diameters may differ from one row to two upwind rows (i.e.  $D_i \neq D_{i-2}$ ), WTs result staggered along  $x$  not only across consecutive, but also across non-consecutive rows. Summarising, an irregularly staggered WT array configuration is implemented. The special case with the same WT model installed all over the WF is also implemented, thus resulting in a uniformly staggered WT array.

Wu et al. [19] demonstrated that, with respect to a reference WF layout with both spatially- and vertically-aligned WTs, the sole lateral staggering with symmetrically-positioned WTs is more efficient than the sole vertical staggering (see layouts “WF2” and “WF6” in Table 1 therein, respectively). Thus, the present WT spatial arrangement is partly similar to the symmetrically laterally-staggered most efficient WF2 layout implemented by Wu et al. [19]. Yet, it is more general than WF2: since herein WTs are concurrently laterally- and vertically-(varying  $H_{hub}$ ) staggered, findings by Wu et al. [19] in arranging WTs either laterally or vertically staggered vs. perfectly aligned are both incorporated, and thus overall WF efficiency is increased.

### 4. Wind farm layout optimization procedure

The WFLO procedure has been addressed based on the flowchart presented in Fig. 5. It is based on two Fortran modules, run in cascade: (i) a layout generator, and (ii) a layout analyser. Pseudocodes of these modules are presented as Algorithm 1 and Algorithm 2 in the supplementary material.

From the WT database all models with  $P_r \geq 500$  kW (Section 3.2) are conditionally ingested by the layout generator. For any WF layout, the module allocates each WT according to both the layout configuration criteria (Section 3.3) and the WT rotor diameter. Creation of each WF layout is terminated when the sum of all WT spacing along both the crosswind ( $x$ ) and downwind ( $y$ ) directions exceeds the WF overall sizes, i.e.  $L_x$  and  $L_y$  (Fig. 4). Module’s final step is the creation of  $N_{WF}$  layouts, each containing – for all installed WTs – the progressive code in the WF (#), the WT database identifier (manufacturer, model, and  $H_{hub}$ ), and the coordinates. Based on data from current case study, a total of  $N_{WF} = 22,721$  layouts were eventually generated: this number includes 6400 layouts by Vestas, 3969 layouts by Nordex, and 2704 layouts by Enercon.

During the second stage, the layout analyser resolves all layouts generated during the previous stage. Based on its database identifier, each WT within any layout is uniquely fetched from the WT database and corresponding characteristics are imported. External information concerning site features, wind conditions, WT- and site-specific losses parameters, and WT cost and plant parameters are also required by the module. The layout analyser implements the  $C_T$  computation as a function of wind speed, wind speed vertical extrapolation, Jensen’s wake model and related losses/efficiency computation, the WT- and site-specific losses computation, the wind energy parameters calculation, and the cost model. For each WT, power losses other than wake losses are calculated through Eqs. (22) and (23): for WT-specific losses (Eq. (22)), the  $f_x$  values reported in Table 3 of [36] as a function of WT system have been used; for site-related losses (Eq. (23)), the following values have been assumed:  $f_{grid} = 2\%$ ;  $f_{ice} = 2\%$ ;  $f_{other} = 0\%$ . As for  $LCoE$ , it was calculated setting in Eq. (29) the following values:  $n = 20$  years;  $d = 5\%$ . Two outputs are ultimately produced: (i) a summary file, including the list of all generated layouts with the overall

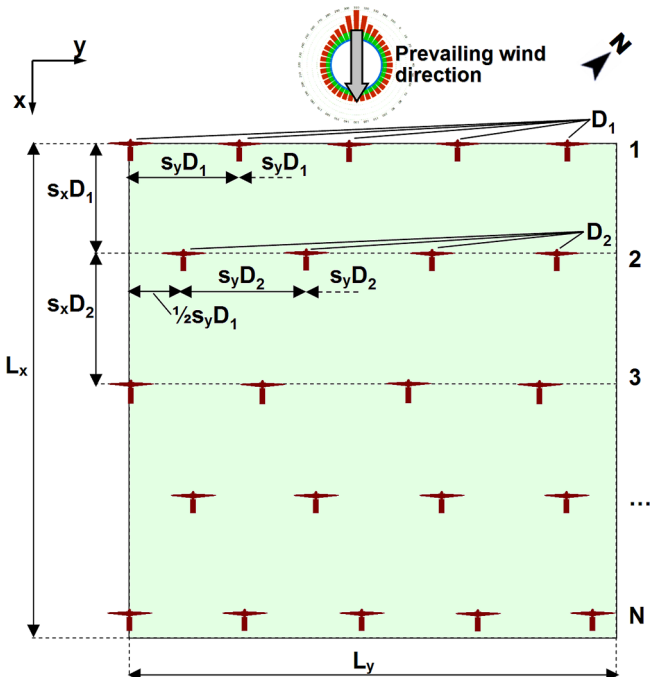
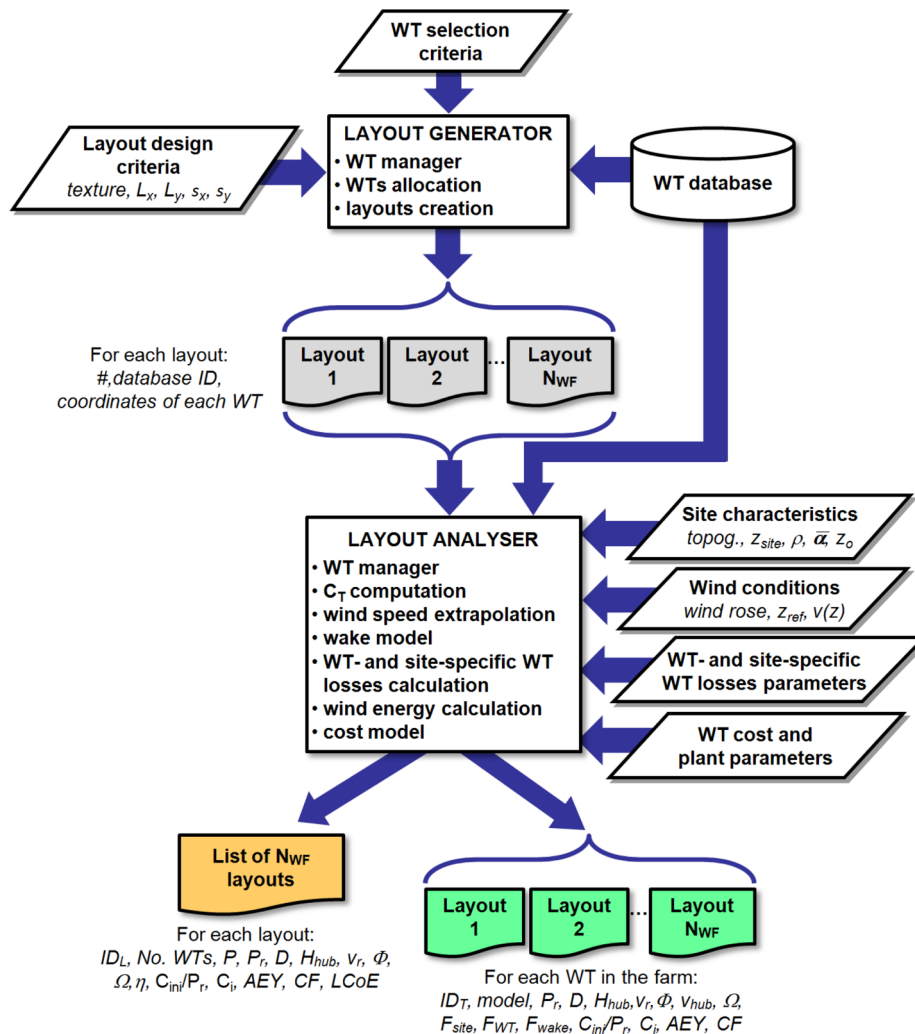


Fig. 4. Design of the irregularly staggered array-based and square ( $L_x = L_y = 2000$  m) WF layout to be optimized. WTs are aligned and equally spaced (same  $\Delta_y$ ) along the crosswind direction  $y$ , while staggered and unequally spaced (different  $\Delta_x$ ) along the downwind direction  $x$ . The same WT is used along  $y$ , while WTs are varied along  $x$ . An initial offset from left-hand side is set for WTs of the even rows. WTs are staggered along  $x$  not only across consecutive, but also across non-consecutive rows. The special case with the same WT installed all over the WF is also implemented. Wind conditions w1 (Fig. 3a) and w0.5 (Fig. 3b) are considered.



**Fig. 5.** Flowchart of the developed WFLO procedure.

characteristics and performances of each ( $N_{WF}$  records); (ii) a number of files, one for any layout, detailing the characteristics and performances of each WT within the WF ( $N_{WF}$  files).

## 5. Results and discussion

A number of analyses have been addressed, aimed at: (i) assessing the most reasonable spacing between the WTs in the farm and WTs operating conditions; (ii) comparing different  $C_T$  estimation methods; (iii) analysing distribution of main WF layout parameters in all generated layout instances; (iv) detecting the optimal WF layouts; (v) investigating WFLO key factors through the SOMs.

### 5.1. Preliminary analysis of wind turbine spacing and wind turbine operating conditions

A preliminary analysis has been addressed in order to calculate the optimal – or, at least, the most reasonable – values of downwind and crosswind spacing to be assigned to WTs, i.e. the values of  $s_x$  and  $s_y$  multipliers of WT rotor diameters (Fig. 4).

In the past literature, the most suitable WT spacing in a WF layout has been long debated. For example, crosswind WT spacing was suggested in the range of 1.5–3 D [34], 3.75 D [19], 2–4 D [53], 3–5 D [54], 4–5 D [4], 5 D [55], 4–8 D [10]. Recommended downwind WT spacing ranges 7 D [19], 7.28 D [25], 4–8 D [10], 5–9 D [54], 8–10 D [55], 8–12 D [53]. In all these works the suggested ranges were inspired

by the goal of minimising WT array losses, i.e. maximising WF efficiency. A more thorough analysis was addressed by Stevens et al. [52] aiming at optimizing further parameters, markedly the normalised power per unit cost, i.e. the reciprocal of  $LCoE$ . Working on flat terrain and using a uniform WT spacing with a single wind direction, they defined a geometric mean WT spacing (combined rotor diameter multiplier) as  $s = \sqrt{s_x s_y}$ : for the case of staggered WF layouts, they suggested an optimal  $s_{opt}$  in the order of 10, while under the same conditions a value of  $s_{opt} = 15$  was suggested by Meyers and Meneveau [56].

To this goal, according to the adopted layout configuration (Fig. 4), a massive computation effort has been made to generate clusters of WF layouts each constructed by varying both crosswind and downwind WT spacing. In particular, for each wind condition, crosswind spacing was varied between 5 and 10 D, while downwind spacing was varied between 7 and 12 D. The result of this analysis is presented in Fig. S2, where for a number of meaningful parameters the distribution median values in all  $N_{WF} = 22,721$  layouts generated within each cluster are plotted.

The number of installed WTs (Fig. S2a) and related power (Fig. S2b) do not change by wind condition, as they are only a function of the WT placement criteria (Section 3.3). The number of WTs clearly reduces as both WT crosswind and downwind distances increase (Fig. S2a), and so does the installed wind power (Fig. S2b). As expected, array efficiency increases with both the downwind ( $s_x$ ) and crosswind ( $s_y$ ) multipliers (Fig. S2c): the increase is appreciable under  $w0.5$  for both  $s_x$  and  $s_y$ , while it is marginal under  $w1$ , particularly if varying  $s_x$ . This  $\eta$  pattern

concurs with the findings from two WFLO studies both based on real wind data, markedly the one addressed by Mirghaed et al. over three sites in Iran [57], and the one addressed by Pookpunt et al. at a site in Thailand [10].

By contrast, in the AEY plot (Fig. S2d) the curves of  $s_x$  for  $w0.5$  are basically flat, while for  $w1$  a relevant decreasing slope is observed for  $s_x$ , which however reduces as  $s_y$  increases. In the CF plot (Fig. S2e), for any wind condition the benefit of placing the WTs as much apart as possible appears basically negligible for both orientations. As for  $LCoE$  (Fig. S2f), it significantly reduces for both wind conditions and WT spacing orientations, yet with an improvement which is higher for  $w0.5$  than  $w1$  condition. These trends of AEY, CF and  $LCoE$  are consistent with those achieved by Pookpunt et al. in Huasai (Thailand), where a similar  $2 \times 2$  km sized layout was used [10].

Following this analysis, optimal  $s_x$  and  $s_y$  values may be theoretically achieved by indefinitely increasing their values, thus agreeing with the findings of  $s_{opt} = 15$  returned by Meyers and Meneveau [56]. However, for practical convenience, thus not excessively reducing the WTs number in the WF, a more reasonable – rather than “optimal” in strictly mathematical terms – value has been chosen for  $s_{opt}$ . Agreeing with suggestions by Stevens et al. [52], a uniform spacing of 10D was set for WT arrays along both wind directions (i.e.  $s_x = s_y = 10$ ).

It is clear that shape, WT spacing and WT spatial arrangement of currently-developed WF layouts strictly depend – besides the  $10D \times 10D$  spacing – on the number and characteristics (i.e.  $D$  and  $H_{hub}$ ) of all available WTs: for example, a minimum of 2 and a maximum of 6 rows were implemented within all generated WF layouts. Also total number of the latter ( $N_{WF} = 22,721$ ) depends on the characteristics of the selected WTs.

A further analysis has been addressed by crossing WT characteristics (Table 2) and wind conditions (Fig. 3). To include all WTs in the statistics, since their large  $H_{hub}$  range of variability (35–164 m, Table 2), all single wind magnitudes have been vertically extrapolated from  $z_{ref}$  to the specific WT  $H_{hub}$ , using the PL with  $\bar{\alpha} = 0.20$ . Furthermore, for simplicity, all free stream wind magnitudes have been considered, thus disregarding any wind deficit possibly affecting the WTs in the WF. The final result of this filtering is summarised in Table S2. Under the  $w0.5$  regime all WTs operate below the rated conditions, and almost all WTs (98.53%) operate above the cut-in wind speed. Under  $w1$  all WTs operate above the cut-in, with a remarkable 66.37% operating at rated conditions and only a remaining 33.63% in the region between  $v_i$  and  $v_r$ .

## 5.2. Comparison among different thrust coefficient estimation methods

The method expressing  $C_T$  as a function of  $C_p$  [21], and the method currently proposed expressing  $C_T$  as a function of  $v$  (Section 2.3) have been compared against the classical approach setting for  $C_T$  a constant 0.88 value. Two “extreme” WF layouts (derived from Section 5.1) have been considered: (i) the “worst” layouts, i.e. using the  $5D \times 7D$  WT spacing; (ii) the “best” layouts, i.e. using the  $10D \times 10D$  WT spacing selected in the present study. The overall scores of this comparison, for each WT spacing and wind condition, are summarised in Table S3 in terms of range and median values achieved for the main WF layout performance parameters.

For the least efficient layouts ( $5D \times 7D$ ), under the lower wind regime ( $w0.5$ ) both  $C_T(C_p)$  and  $C_T(v)$  methods return more optimistic median values than does the  $C_T = 0.88$  method, with  $C_T(C_p)$  being more optimistic than  $C_T(v)$ . In particular, an over-estimation of 6.6% for  $\eta$  and an under-estimation of 3.9% for  $LCoE$  are returned by  $C_T(C_p)$ , while more conservative scores (1.2% over-estimation for  $\eta$  and 0.7% under-estimation for  $LCoE$ ) are returned by  $C_T(v)$ . Under the higher wind regime ( $w1$ ), the  $C_T(C_p)$  method is more pessimistic than the  $C_T = 0.88$  method, as  $C_T$  is estimated as such that the median values of  $\eta$  are under-estimated by 2.6% and  $LCoE$  under-estimated by 0.2%. By contrast, the  $C_T(v)$  method is more optimistic than the fixed method, as  $\eta$  is

over-estimated by 6.3% and  $LCoE$  under-estimated by 0.2%. If analysing the reported ranges for the objective functions, both  $CF$  maxima and  $LCoE$  minima are unchanged under the  $w1$  regime, and differ by a small amount under the  $w0.5$  regime. Qualitatively the same conclusions may be drawn when considering the most efficient layouts ( $10D \times 10D$ ), though with smaller overall differences:  $LCoE$  median values are at most under-estimated by 1.3% by  $C_T(C_p)$  and 0.3% by  $C_T(v)$ , while both  $CF$  maxima and  $LCoE$  minima remain basically unchanged.

The scores currently achieved for the  $C_T(v)$  method are consistent with the remarks by Feng et al. [23]. Comparing the typical shapes of the  $C_T$  curve and power curve provided by manufacturers, they concluded that wake effects among WTs are more critical in the WT operating region between  $v_i$  and  $v_r$ , while not so serious above  $v_r$ . If considering the fractions of WTs operating in the  $v_i-v_r$  region under  $w0.5$  and  $w1$  (98.53 vs. 33.63%, Table S2), this accounts for the fact that lower efficiency (higher wake losses) are estimated by  $C_T(v)$  for  $w0.5$  than  $w1$  (both for  $5D \times 7D$  and  $10D \times 10D$  arrays), while – unrealistically – no difference results if applying the  $C_T = 0.88$  method. This also confirms recommendations by Feng et al. [23] that especially for WFs built on “poor” wind sites, WFLO must play an important role.

Overall, since both alternative methods return  $C_T$  as a function of the full range of either  $C_p$  or  $v$ , their use should be preferred to the fixed method as allowing to more accurately reproducing the wake interactions among WTs whatever the specific WT spacing or wind conditions affecting the WF. Among them, the  $C_T(v)$  method appears as more robust and easier to be applied.

## 5.3. Parameters distribution in all generated wind farm layouts

After processing all generated WF layouts, in the supplementary material the kernel density plots of main WF layout parameters are presented, either independent (Fig. S3) or dependent (Fig. S4) on wind conditions. They have been achieved by applying the “sm.density.compare” function [58] of the “sm” R package [59]. Since returning the overall variation range of each parameter, such plots are key to assess the “tuning range” of each WF design parameters and how they may impact on WF performance parameters.

As for the wind-independent parameters, while two peaks appear in the density plot of number of WTs (Fig. S3a) and site- and WT-related losses (Fig. S3f), the distribution of the other parameters generally exhibits a single peak, wider for  $P_r$  (Fig. S3b),  $D$  (Fig. S3c),  $H_{hub}$  (Fig. S3d), and  $C_{inj}/P_r$  (Fig. S3g), and narrower for  $\phi$  (Fig. S3e). The latter distributions are generally skewed to the left (lower values) except for  $D$  and  $H_{hub}$ , roughly centred on the mean of the sample.

In the  $\Omega$  density plot (Fig. S4a), two peaks appear as a function of wind condition, taller and narrower the one related to  $w0.5$  (roughly centred on 50%), shorter and wider the one related to  $w1$  (roughly centred on 95%). As expected, the  $\eta$  density plot (Fig. S4b) for  $w1$  is narrowly peaked around values close to 100%, while surprisingly the distribution for  $w0.5$  exhibits two peaks, one centred on 98%, and the other on 100%. The density plot of array wake losses (Fig. S4c) is clearly the mirrored  $\eta$  density plot (Fig. S4b).

As widely expected, the selected wind condition plays a pivotal role in the density plots of total power losses (Fig. S4d),  $C_i$  (Fig. S4e), AEY (Fig. S4f), CF (Fig. S4g), and  $LCoE$  (Fig. S4h): distributions are more peaked for  $w0.5$ -linked  $C_i$  and AEY, and  $w1$ -linked total losses, CF and  $LCoE$ , while wider for the remaining cases. Noteworthy, since  $C_i$  is a linear function of AEY – as well as of  $P_r$  (see Section 2.4) –, density plot of  $C_i$  almost match the AEY one: the two distributions are very strongly correlated ( $r = 0.996$ ). Overall, Fig. S4 shows that a limited variation range affects the objective functions  $LCoE$  and CF under  $w1$ , while this is far larger under the lower  $w0.5$  regime, when therefore the WF design criteria appear a more critical issue to be addressed.

#### 5.4. Search for optimal wind farm layout

In Table 3 the characteristics of layouts maximising *CF* (L1 and L2) and minimising *LCoE* (L3 and L4) are summarised as a function of wind case study. Characteristics and performances of WTs within each layout are detailed in Tables 4 and 5, while their placement is depicted in Fig. 6.

When wind condition *w0.5* occurs, a maximum *CF* of 46.22% is achieved by layout L1 (Table 3), employing 4 W2E WTs for an overall 8000-kW installed power (Table 4 and Fig. 6a). Accordingly, a minimum *LCoE* of 143.44 \$/MWh is obtained by layout L3 (Table 3), which is made up of 9 Leitwind WTs summing up 7,200-kW capacity (Table 5 and Fig. 6c). However, since *LCoE* for layout L1 is basically the same as L3 (143.47 \$/MWh), L1 may be considered as the optimal layout in that both optimization functions are satisfied. For the wind case study *w1*, *CF* is maximised to 92.17% by layout L2 (Table 3) that employs 4 W2E WTs amassing 8000-kW installed power (Table 4 and Fig. 6b), while *LCoE* is minimised to 103.46 \$/MWh by layout L4 (Table 3) using 9 Leitwind WTs totalling 7200-kW capacity (Table 5 and Fig. 6c). In this case, layout L4 should be preferred as *LCoE* is minimised and a remarkable *CF* = 88.23% is achieved as well.

Within a survey worldwide updated to the year 2017, IRENA [38] reported typical *LCoE* ranges for onshore wind projects as a function of project's size: for the installed capacities involved in the current study (about 7–30 MW), they reported *LCoE* values ranging between a minimum of 40–50 and a maximum of 150–180 \$/MWh, which basically encompass the *LCoE* values achieved in this study. The minimum *LCoE* currently achieved for *w0.5* (143.44 \$/MWh) is in general agreement with the values reported by Pookpunt et al. [10]. Using the same NREL cost model and assuming a similar 2 × 2 km sized layout with uniform WT spacing, for a real wind case in Huasai (Thailand) they analysed *LCoE* variation as a function of WT spacing and rated power, returning for 8D × 8D spacing and  $P_r = 660$ –3000 kW *LCoE* values ranging 137.20–164.80 \$/MWh. This outcome was achieved for  $v_m = 4.42$  m/s observed at 40 m, while at the same height for *w0.5* it is currently  $v_m = 6.45$  m/s.

Conversely, present minimum *LCoE* values are higher than those reported by Mirghaed et al. [57]. Again based on the NREL cost model and on observed wind data, they designed square layouts sized  $1.73 \times 1.73$  km over the sites of Khaf (40-m  $v_m = 10.5$  m/s) and Ahar (40-m  $v_m = 8.91$  m/s) in Iran: using downwind/crosswind WT spacing of 6D × 3D and 5D × 3D, respectively, they achieved corresponding *LCoE* values of 55 and 67.2 \$/MWh, which are lower than *LCoE* = 103.46 \$/MWh currently achieved for *w1* wind condition (40-m  $v_m = 12.9$  m/s).

From Tables 4 and 5, it should be noted that all optimal layouts are made up of identical WTs, (i.e. same model and same  $H_{hub}$ ), with the only exception of layout L2 (employing 2 different WT models). In particular, for layouts L1, L3 and L4 there is only one combination of  $P_r$ ,  $D$  and  $H_{hub}$  ( $N_p = N_D = N_H = 1$ ), while for layout L2 the only variation involves  $D$  ( $N_p = N_H = 1$ ,  $N_D = 2$ ). Furthermore, using the same 9 Leitwind models results in *LCoE* minimisation under both wind case studies (Table 5): corresponding layouts are identical (Fig. 6c) except for in L4  $H_{hub}$  is lower (61.5 m) than in L3 (80 m). Also, for both optimization conditions a higher WF-averaged  $H_{hub}$  is needed for layouts facing the weaker (*w0.5*) than the stronger (*w1*) wind conditions (Table 3). This outcome agrees with findings by Mirghaed et al. [57] that regions with higher  $v_m$  have lower optimal ratio of  $H_{hub}$  to both  $D$  and  $P_r$ . Findings by Gualtieri [36] that minimum *LCoE* is achieved at lower  $H_{hub}$  (61.5–80 m) than maximum *CF* (100–140 m) are also confirmed.

If comparing the *w1*-related layouts (Table 3), *LCoE* for L4 is lower than for L2 because of the lower annual cost (706 vs. 814 \$/kW/y), although the initial capital cost is higher (1878 vs. 1823 \$/kW) and *CF* is lower (88.23 vs. 92.17%). In terms of efficiency, layouts comprising 4 WTs (L1 and L2) returned no wake losses ( $\eta = 100\%$ , Table 3), while a

**Table 4**  
Details of WF layouts maximising *CF* by wind case study. WTs placement in WF layouts is depicted in Fig. 6a (L1) and Fig. 6b (L2).<sup>a,b</sup>

| WF layout | Wind case study | WT | $P_r$ (kW)        | $H_{hub}$ (m) | $v_r$ (m/s) | $\phi = v_r/v_t$ | $v_{hub}$ (m/s) | $\Omega = v_m/v_r$ (%) | Losses (%) | #                                      | Model                  | Site                    | WT     | Array wake |        |        |       |
|-----------|-----------------|----|-------------------|---------------|-------------|------------------|-----------------|------------------------|------------|--|------------------------|-------------------------|--------|------------|--------|--------|-------|
|           |                 |    |                   |               |             |                  |                 |                        |            | C <sub>m</sub> /P <sub>r</sub> (\$/kW) | C <sub>t</sub> (\$/kW) | A <sub>EY</sub> (MWh/y) | CF (%) |            |        |        |       |
| L1        | <i>w0.5</i>     | 1  | W2E Harvester 2.0 | 2,000         | 116         | 140              | 10              | 2.90                   | 7.11       | 71.10                                  | 3.97                   | 6.36                    | 0      | 2,309      | 116.35 | 8,097  | 46.22 |
|           |                 | 2  | W2E Harvester 2.0 | 2,000         | 116         | 140              | 10              | 2.90                   | 7.11       | 71.10                                  | 3.97                   | 6.36                    | 0      | 2,309      | 116.35 | 8,097  | 46.22 |
|           |                 | 3  | W2E Harvester 2.0 | 2,000         | 116         | 140              | 10              | 2.90                   | 7.11       | 71.10                                  | 3.97                   | 6.36                    | 0      | 2,309      | 116.35 | 8,097  | 46.22 |
|           |                 | 4  | W2E Harvester 2.0 | 2,000         | 116         | 140              | 10              | 2.90                   | 7.11       | 71.10                                  | 3.97                   | 6.36                    | 0      | 2,309      | 116.35 | 8,097  | 46.22 |
| L2        | <i>w1</i>       | 1  | W2E Harvester 2.0 | 2,000         | 116         | 100              | 10              | 2.90                   | 14.22      | 142.20                                 | 3.97                   | 6.36                    | 0      | 2,095      | 203.52 | 16,149 | 92.17 |
|           |                 | 2  | W2E Harvester 2.0 | 2,000         | 116         | 100              | 10              | 2.90                   | 14.22      | 142.20                                 | 3.97                   | 6.36                    | 0      | 2,095      | 203.52 | 16,149 | 92.17 |
|           |                 | 3  | W2E 93–2.0        | 2,000         | 93          | 100              | 12.5            | 3.60                   | 14.22      | 113.76                                 | 3.97                   | 6.36                    | 0      | 1,551      | 203.52 | 16,149 | 92.17 |
|           |                 | 4  | W2E 93–2.0        | 2,000         | 93          | 100              | 12.5            | 3.60                   | 14.22      | 113.76                                 | 3.97                   | 6.36                    | 0      | 1,551      | 203.52 | 16,149 | 92.17 |

<sup>a</sup> Layouts were built-up as in Fig. 4 with 10D × 10D WT spacing.

<sup>b</sup> Number of different WT combinations per layout:  $N_p = N_D = N_H = 1$  (L1);  $N_p = N_H = 1$ ,  $N_D = 2$  (L2).

**Table 5**  
Details of WF layouts minimising LCoE by wind case study. WTs placement in WF layouts is depicted in Fig. 6c (L3 & L4).<sup>a,b</sup>

| WF layout | Wind case study | WT | $P_r$ (kW)         | $H_{hub}$ (m) | $D$ (m) | $\nu_r$ (m/s) | $\phi = \nu_r/\nu_i$ | $\nu_{hub}$ (m/s) | $\Omega = \nu_m/\nu_i$ (%) | Losses (%) | $C_m/P_r$ (\$/kW) |       | $C_i$ (\$/kW) | AEY (MWh/y) | CF (%)     |       |
|-----------|-----------------|----|--------------------|---------------|---------|---------------|----------------------|-------------------|----------------------------|------------|-------------------|-------|---------------|-------------|------------|-------|
|           |                 |    |                    |               |         |               |                      |                   |                            |            | #                 | Model | Site          | WT          | Array wake |       |
| L3        | w0.5            | 1  | Leitwind LTW77-800 | 800           | 76.7    | 80            | 11                   | 3.70              | 7.14                       | 64.91      | 3.97              | 8.13  | 0             | 1996        | 38.86      | 25.29 |
|           |                 | 2  | Leitwind LTW77-800 | 800           | 76.7    | 80            | 11                   | 3.70              | 7.14                       | 64.91      | 3.97              | 8.13  | 0             | 1996        | 38.86      | 25.29 |
|           |                 | 3  | Leitwind LTW77-800 | 800           | 76.7    | 80            | 11                   | 3.70              | 7.14                       | 64.91      | 3.97              | 8.13  | 0             | 1996        | 38.86      | 25.29 |
|           |                 | 4  | Leitwind LTW77-800 | 800           | 76.7    | 80            | 11                   | 3.70              | 7.14                       | 64.91      | 3.97              | 8.13  | 0             | 1996        | 38.86      | 25.29 |
|           |                 | 5  | Leitwind LTW77-800 | 800           | 76.7    | 80            | 11                   | 3.70              | 7.20                       | 56.36      | 3.97              | 8.13  | 0             | 1996        | 38.86      | 25.29 |
|           |                 | 6  | Leitwind LTW77-800 | 800           | 76.7    | 80            | 11                   | 3.70              | 6.20                       | 56.36      | 3.97              | 8.13  | 0             | 1996        | 38.86      | 25.29 |
|           |                 | 7  | Leitwind LTW77-800 | 800           | 76.7    | 80            | 11                   | 3.70              | 6.36                       | 57.82      | 3.97              | 8.13  | 5.33          | 1996        | 37.28      | 23.84 |
|           |                 | 8  | Leitwind LTW77-800 | 800           | 76.7    | 80            | 11                   | 3.70              | 5.71                       | 51.91      | 3.97              | 8.13  | 5.33          | 1996        | 37.28      | 23.84 |
|           |                 | 9  | Leitwind LTW77-800 | 800           | 76.7    | 80            | 11                   | 3.70              | 5.98                       | 54.36      | 3.97              | 8.13  | 5.33          | 1996        | 37.28      | 23.84 |
| L4        | w1              | 1  | Leitwind LTW77-800 | 800           | 76.7    | 61.5          | 11                   | 3.70              | 14.28                      | 129.82     | 3.97              | 8.13  | 0             | 1878        | 78.41      | 61.83 |
|           |                 | 2  | Leitwind LTW77-800 | 800           | 76.7    | 61.5          | 11                   | 3.70              | 14.28                      | 129.82     | 3.97              | 8.13  | 0             | 1878        | 78.41      | 61.83 |
|           |                 | 3  | Leitwind LTW77-800 | 800           | 76.7    | 61.5          | 11                   | 3.70              | 14.28                      | 129.82     | 3.97              | 8.13  | 0             | 1878        | 78.41      | 61.83 |
|           |                 | 4  | Leitwind LTW77-800 | 800           | 76.7    | 61.5          | 11                   | 3.70              | 14.28                      | 129.82     | 3.97              | 8.13  | 0             | 1878        | 78.41      | 61.83 |
|           |                 | 5  | Leitwind LTW77-800 | 800           | 76.7    | 61.5          | 11                   | 3.70              | 12.64                      | 114.91     | 3.97              | 8.13  | 0             | 1878        | 78.41      | 61.83 |
|           |                 | 6  | Leitwind LTW77-800 | 800           | 76.7    | 61.5          | 11                   | 3.70              | 12.64                      | 114.91     | 3.97              | 8.13  | 0             | 1878        | 78.41      | 61.83 |
|           |                 | 7  | Leitwind LTW77-800 | 800           | 76.7    | 61.5          | 11                   | 3.70              | 12.71                      | 115.55     | 3.97              | 8.13  | 1.33          | 1878        | 78.41      | 61.83 |
|           |                 | 8  | Leitwind LTW77-800 | 800           | 76.7    | 61.5          | 11                   | 3.70              | 11.90                      | 108.18     | 3.97              | 8.13  | 1.33          | 1878        | 78.41      | 61.83 |
|           |                 | 9  | Leitwind LTW77-800 | 800           | 76.7    | 61.5          | 11                   | 3.70              | 12.14                      | 110.36     | 3.97              | 8.13  | 1.33          | 1878        | 78.41      | 61.83 |

<sup>a</sup> Layouts were built-up as in Fig. 4 with 10D × 10D WT spacing.

<sup>b</sup> Number of different WT combinations per layout:  $N_p = N_D = N_H = 1$  (L3 & L4).

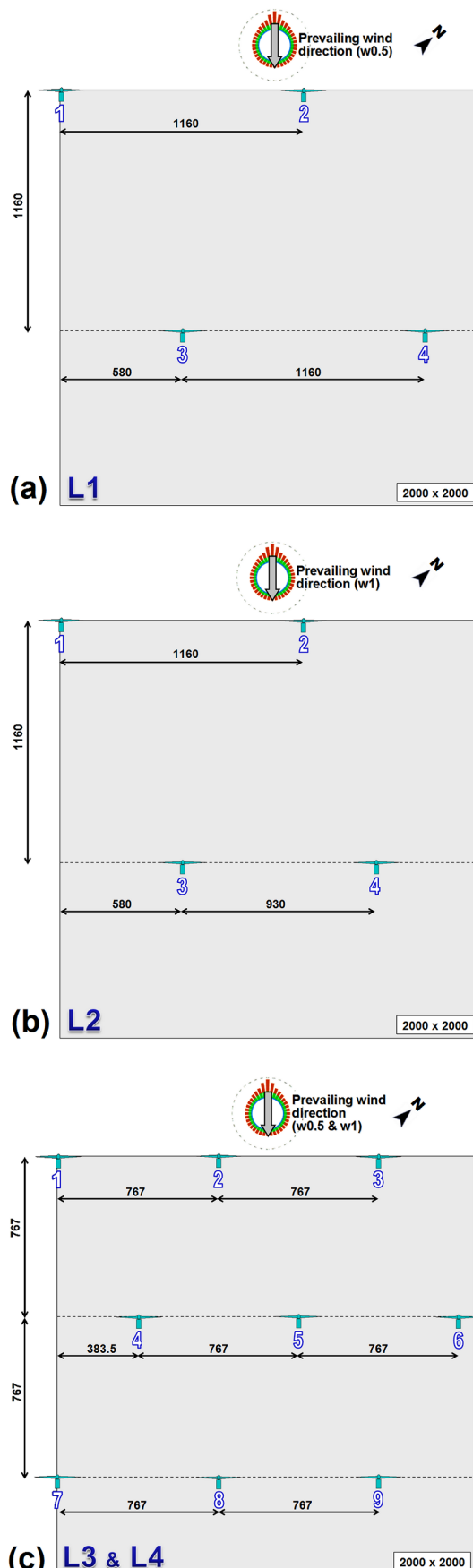


**Fig. 6.** Sketch of optimal WF layouts: (a) maximising  $CF$  for  $w0.5$  (L1); (b) maximising  $CF$  for  $w1$  (L2); (c) minimising  $LCoE$  for both  $w0.5$  and  $w1$  (L3 & L4). WT numbers refer to the list given in Table 4 for layouts L1 and L2, and in Table 5 for layouts L3 and L4. Layouts L3 and L4 are identical except for in L4 WT  $H_{hub}$  is lower (61.5 m) than in L3 (80 m). Layouts were built-up as in Fig. 4 with  $10D \times 10D$  WT spacing. Measures are in meter.

certain losses were observed for 9-wt layouts (L3 and L4) mostly as a result of wake losses involving WTs of the last row (Table 5 and Fig. 6c). When wind regime  $w1$  occurs (L2 and L4), the mean wind magnitude blowing at WT  $H_{hub}$  ( $v_{hub}$ ) is always higher than corresponding  $v_r$ , meaning that the  $\Omega$  parameter is always above 100% (Tables 4 and 5), even for WTs subject to wake losses (WTs nos. 7, 8, and 9 of L4, Table 5). It should be also noted that, given the commercial WT portfolio at disposal, the average  $v_r$  values of the optimal WF layouts are close to the minimum of the  $v_r$  range (10–18 m/s) given in Table 2 and plotted in Fig. S1e: 10–11.25 m/s for maximising  $CF$ , and 11 m/s for minimising  $LCoE$  (Table 3).

### 5.5. Investigation on key factors through the self-organizing maps

For each wind case study, the SOM algorithm was applied to the full dataset of  $N_{WF} = 22,721$  layouts for the following variables: No. WTs,  $N_p$ ,  $N_D$ ,  $N_H$ ,  $P$ ,  $P_r$ ,  $D$ ,  $H_{hub}$ ,  $v_r$ ,  $\Phi$ ,  $\Omega$ ,  $\eta$ ,  $C_{ini}/P_r$ , AEY,  $CF$ , and  $LCoE$ . The SOMs were visualized by component planes represented by the above variables. To avoid redundancy, those variables whose distribution was strictly correlated to the others were withdrawn, as was the case of  $C_i$ : since strongly correlated to AEY ( $r = 0.996$ ), the SOM component plane of  $C_i$  should be considered the same as AEY. After a 10,000-iteration training, the final SOM structure was established on two layers of neurons, i.e.: (i) an input layer, consisting of a number of neurons (22,721) corresponding to the layouts of the above-selected 16 variables; (ii) an output layer, consisting of 100 neurons, visualized by hexagons, organized in 2-D grids with 10 rows and 10 columns. The result of SOM application is presented in Fig. 7 (wind condition  $w1$ ), and Fig. 8 ( $w0.5$ ). The free and open-source Living for SOM tool (<http://livingforsom.com>) was used for all SOM computations.

As shown in Fig. 7, for a remarkable wind potential site ( $w1$  regime) SOM topology of  $LCoE$  is significantly different from  $CF$  topology, as max-to-min orientation of the former is from top-right (TR) to top-left (TL) of map's corner, while min-to-max orientation of the latter is bottom-right (BR) to TR. The two topologies are not mirrored, meaning that increasing  $CF$  does not necessarily result in decreasing  $LCoE$ . This outcome concurs with the one achieved within a WT optimal site matching addressed at the FINO3 offshore platform (Germany) [36]: although an offshore site, FINO3 was a “superb” site (50-m  $v_m = 9.71$  m/s) such as a  $w1$  onshore site. Min-to-max oriented SOM topology of  $CF$  is similar to those of  $D$ ,  $\Omega$ ,  $\eta$ ,  $C_{ini}/P_r$  and (mirrored) No. WTs,  $N_H$  and  $v_r$ , meaning that increasing (decreasing for No. WTs,  $N_H$  and  $v_r$ ) the values of such variables leads to an increase of  $CF$ , but not necessarily to a concurrent decrease of  $LCoE$ . SOM clustering of  $LCoE$  is apparently similar to the one of  $P$ , meaning that a way to minimise  $LCoE$  is reducing the overall WF capacity. Although the association is weaker,  $LCoE$  could be minimised by reducing AEY: for a high potential site it is therefore quite surprising that the WFLO may be accomplished by decreasing the overall energy output. At WF-level, as shown by the SOM clustering of No. WTs,  $N_p$ ,  $N_D$  and  $N_H$  for decreasing  $LCoE$  it is required to minimise the total number of WTs as well as the use of WTs with different  $P_r$ ,  $D$  or  $H_{hub}$ . In terms of WT regulation, minimum values of  $v_r$  and quite low values of  $\Phi$  are required: this confirms that reducing  $v_r$  is beneficial as the fraction of WTs working at rated conditions (43.17%, Table S3) increases; as for  $\Phi$ , this outcome was expected following the quite small fraction of WTs operating in the range  $v_r - v_r$  (56.83%, Table S3). Relative maxima of  $P_r$  and  $H_{hub}$  are associated to both minima and maxima of  $LCoE$ , meaning that their influence on

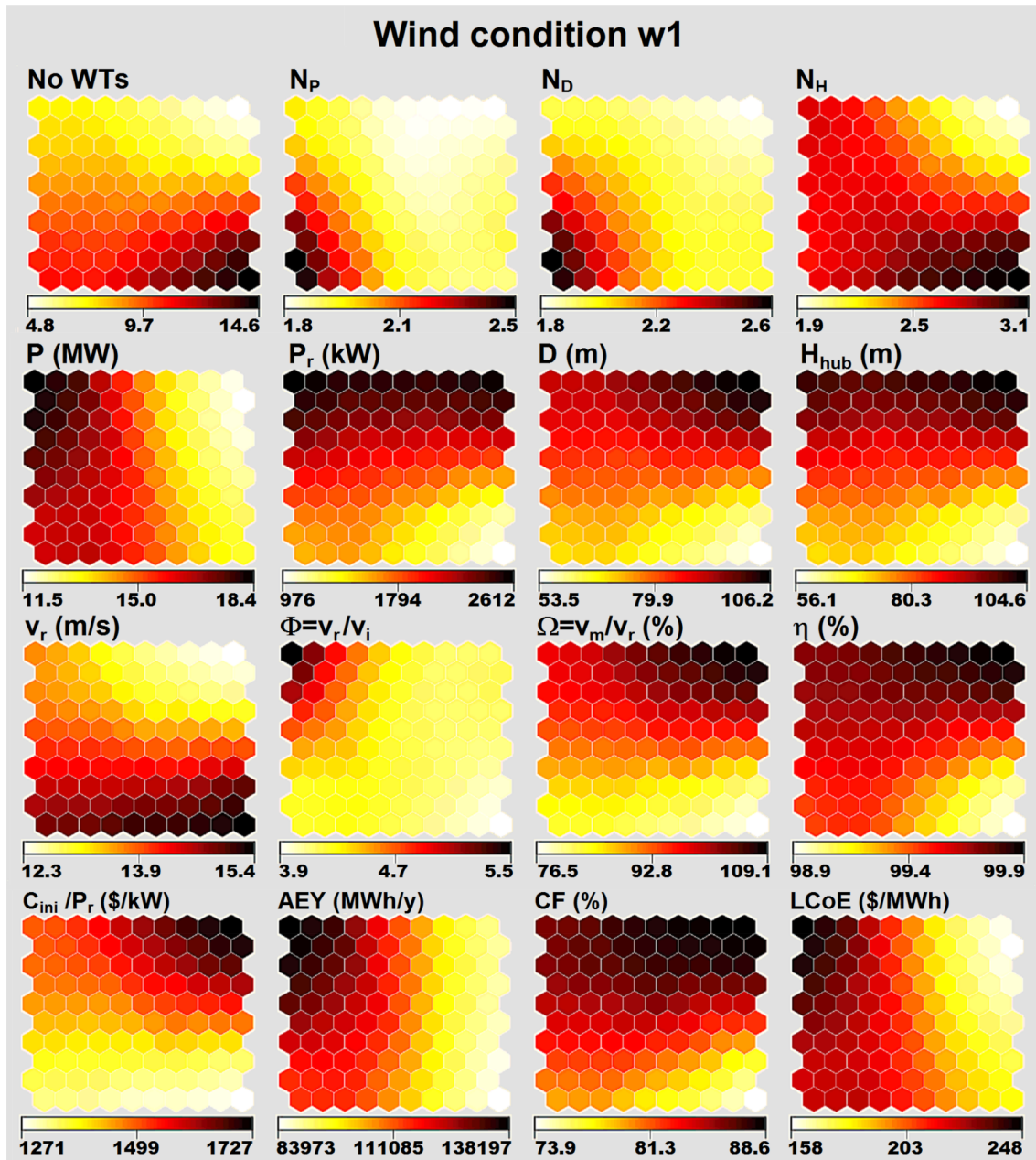


**Fig. 7.** SOM component planes for wind condition  $w1$  obtained for the following WF parameters: WF layout (No. WTs,  $N_p$ ,  $N_d$ ,  $N_h$  and  $P$ ); WT design ( $P_r$ ,  $D$ ,  $H_{hub}$ ,  $v_r$  and  $\Phi$ ); energetic ( $\Omega$  and  $\eta$ ); cost ( $C_{ini}/P_r$ ); energy output (AEY and CF); profitability ( $LCoE$ ). Cumulated values are plotted for WF layout parameters and  $LCoE$ , while the WF-averaged values for all other parameters. A total of 22,721 layouts built-up as in Fig. 4 with  $10D \times 10D$  WT spacing were processed. The 16 panels are linked by position as such that the hexagons in a given position correspond to the same map unit.

$LCoE$  is not univocal. Therefore, some findings by Chen et al. [2] are confirmed that  $v_r$  has a larger influence on  $LCoE$  than  $P_r$ , and that a larger WT does not necessarily bring a lower  $LCoE$ . Conversely, their suggestions that wind sites with higher  $v_m$  require higher  $v_r$  are contradicted. In addition, findings by Abdulrahman and Wood [21] are confirmed that, in selecting WTs having the same  $P_r$ , those with larger  $D$  combined with lower  $v_r$  should be prioritised. Interestingly, the fact that  $\Omega$  is basically arranged such as  $CF$  proves that this parameter could be used as an efficient metric to assess the overall WF layout performances. As expected, the highest energy production is achieved by maximising the WF capacity, while not particularly expensive WTs and energetically efficient layouts are required to. By contrast, the most costly WTs whose  $v_r$  largely exceeds site's  $v_m$  surprisingly result in quite low AEY. Furthermore, maximum WF energy production is obtained by the least economically viable WF layouts.

For a mid-potential site ( $w0.5$  regime, Fig. 8), the topology of SOM component planes for the objective functions  $CF$  and  $LCoE$  are basically perfectly mirrored, with min-to-max orientation of  $CF$  (TR to bottom-left, BL) quite matching max-to-min orientation of  $LCoE$ . This confirms the results achieved for  $w0.5$ -related layout L1, which concurrently satisfies  $CF$  maximisation and  $LCoE$  minimisation (Table 3). The equivalence between the two optimization functions for mid-potential sites confirms findings by various Authors (e.g. [10]). Compared to  $CF$  – or, mirrored, to  $LCoE$  –, a similar SOM topology affects  $P_r$ ,  $D$ ,  $H_{hub}$ ,  $\Omega$ ,  $C_{ini}/P_r$  (same min-to-max orientation), and (mirrored) No. WTs and  $v_r$  (same max-to-min orientation), meaning that WFLO may be achieved by either maximising the former or minimising the latter variables. Incidentally, most effectively than for the  $w1$  case (Fig. 7), the use of WTs with lower  $P_r$  worsens the WFLO, thus confirming that setting a lower  $P_r$  threshold (500 kW) in the selected WTs (Section 3.2) is a

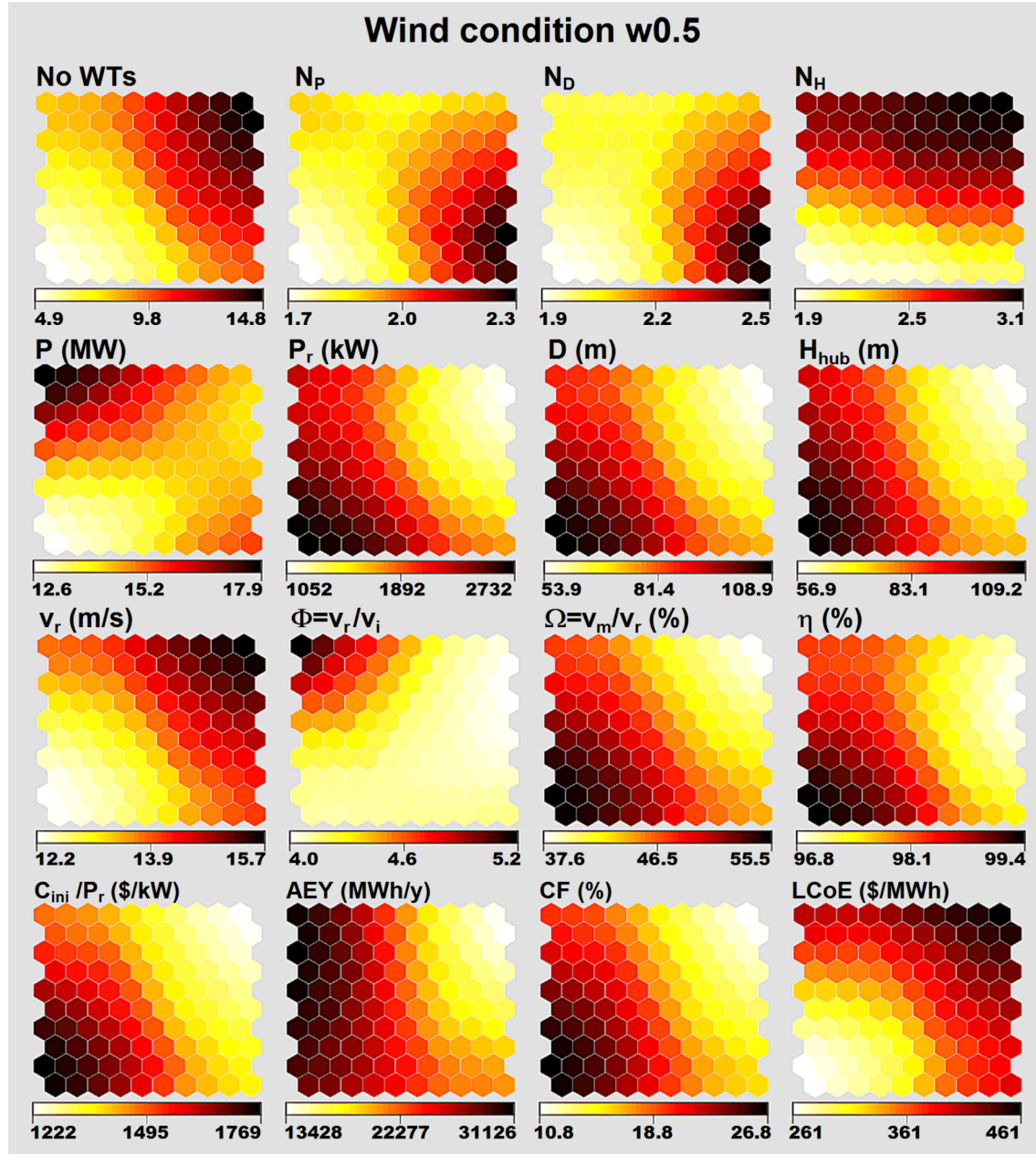


Fig. 8. Same as Fig. 7, but for wind condition w0.5.

reasonable choice. At WF-level, again – as anticipated in Section 5.4 for layouts L1 (Table 4) and L3 (Table 5) – for decreasing *LCoE* it is required to avoid the use of WTs with different  $P_r$ ,  $D$  or  $H_{hub}$  (see SOMs of  $N_p$ ,  $N_d$  and  $N_h$ ). This outcome contrasts with findings, e.g., by Abdulrahman and Wood [21], who suggested being economically preferable a suitable combination of different types of WTs than using identical WTs, particularly as concerns  $H_{hub}$ . Since the number of possible WT combinations in the WF reduces to one combination for each model provided by each manufacturer (i.e. the same WT installed throughout the WF), the specific criteria set for WF layout design (Section 3.3) are useless, and so could be implementing and exploring possible further WT groupings in the WF. Although exhibiting a narrow range between minima and maxima, also  $\eta$  clustering is quite similar to those of both  $CF$  and (mirrored)  $LCoE$ : consistently with the literature (e.g. [6]), this confirms that array efficiency is a meaningful WFLO objective function. As for  $\Phi$ , there is not a univocal result delivered by the corresponding SOM, as lower  $\Phi$  values are associated to both higher (TR neurons) and

lower (BL neurons)  $LCoE$  values: this outcome was somehow expected if considering the remarkable fraction of WTs operating in the range  $v_r-v_i$  (89.77%, Table S3). Current  $\Phi$ -related outcomes agree with Pallabazzer [35] in that increasing  $\Phi$  results in a concurrent increase of both  $AEY$  and  $\eta$ . As for WF minimum/maximum energy production, associations basically similar to those relative to the *w1* case are achieved, except for maximum WF energy production is not associated to the highest  $LCoE$ .

Several multi-variable analyses have been performed in the literature attempting to detect those variables mostly influencing WT or WF optimization. For example, Vasel-Be-Hagh and Archer [60], MirHassani and Yarahmadi [5], and Wu et al. [19] analysed the effect of varying  $H_{hub}$  in order to maximise the  $AEY$  achieved from a WF. Chen et al. [2] addressed a 3-variable analysis (among  $LCoE$ ,  $P_r$  and  $v_r$ ) to detect the exact optimization point which minimises  $LCoE$ . The same goal was pursued by Mirghaed et al. [57] through variation of  $D$ ,  $H_{hub}$ , and  $P_r$ : for a WF over “superb” wind potential sites ( $v_m$  in the order of 10 m/s at 50 m),  $LCoE$  minimisation is suggested by using WTs with

$P_r = 1\text{--}2 \text{ MW}$ . Pookpunt et al. [10] analysed all main WF-affecting parameters, including  $P$ , No. WTs,  $P_r$ ,  $\eta$ ,  $CF$ ,  $AEY$ , and  $LCoE$ : over marginal wind potential sites ( $v_m$  in the order of 5 m/s at 50 m) they suggested a wider  $P_r$  range (660–2600 kW) than Mirghaed et al. [57]. Abdulrahman and Wood [21] analysed the combined variation of  $P_r$ ,  $CF$  and  $LCoE$ , concluding that to minimise  $LCoE$  smaller to medium size WTs with low  $H_{hub}$  should be used. It is clear that the SOMs allow to overcome these and other similar multi-variable investigations. Since capable of retaining the mutual relationships among all analysed variables and disclosing them through a single, compact plot, they are a much more powerful means to straightforwardly derive a WFLO comprehensive pattern, particularly if considering the number and complexity of all variables involved. The SOMs largely improve the WFLO analysis also in the present work. For each parameter in the generated layouts, the kernel density plots analysed in Section 5.3 (Figs. S3 and S4) only allow to assess parameters' full range of variability, but are unable to give any information on the way the pattern for each parameter – and, specifically, their minima/maxima – relate to each other, which conversely the SOMs are capable of. Furthermore – and maybe most importantly –, the SOMs allow to efficiently manage those WFLO problems which involve multiple objective functions, such as the case of Abdulrahman and Wood [21], where power output,  $CF$  and  $LCoE$  were targeted altogether. The SOMs are also capable of coping with the non-convex nature of the WFLO problem: since those variables selected as objective functions are clustered, too, the SOMs do allow to clearly detect global rather than local optimal solutions.

## 6. Conclusions

In this study, a novel method is proposed to optimize an array-based onshore WF layout design based on the characteristics of all commercial-scale WTs. A huge number of overall WT combinations (577) was processed, the highest among all WFLO literature studies. A thorough WFLO analysis was performed through the SOMs: since well capable of coping with all main issues affecting the WFLO problem, they proved a powerful means to straightforwardly achieve a WFLO comprehensive pattern, providing further insights into those parameters (both at WT- and WF-level) that mostly influence the WFLO.

Further key-points of the study include:

- an irregularly staggered WT array design was assumed following literature key findings;
- a preliminary analysis of the most reasonable downwind and crosswind WT spacing was addressed;
- WF layout instances were developed by varying main WT characteristics, including  $P_r$ ,  $D$  and  $H_{hub}$ ;
- a novel formulation was developed to deliver a  $C_T$  experimental curve as a function of wind speed;
- for any WT, not theoretical (approximated or fitted), but experimental power curves were considered;
- the detailed and comprehensive NREL cost model expressing WT cost as a function of  $D$ ,  $P_r$ ,  $H_{hub}$  and  $AEY$  was used;
- a new metric, quantifying the fraction of site's mean wind speed the WT is capable of satisfying when working at rated conditions ( $\Omega = v_m/v_r$ ), was introduced to better assess WF performances;
- the remarkable WT combinations implemented resulted in a huge number of generated WF layouts to be optimized (22,721);
- an analytic method for assessing all power losses other than wake losses was used; since taking WT system type into account, this method provides a further WT distinction by WT characteristics;
- wind magnitude was vertically adjusted to each WT  $H_{hub}$  based on the PL;
- $LCoE$  was selected as primary while  $CF$  as secondary WFLO objective function, and their mutual relationship investigated.

Following the WFLO analysis, a number of recommendations may

be drawn:

- it is confirmed that WF array efficiency is a meaningful objective function, although to a lesser extent than  $CF$  and particularly  $LCoE$ ;
- in general, maximising  $CF$  and minimising  $LCoE$  basically match; for higher wind potential sites, however, increasing  $CF$  does not necessarily result in decreasing  $LCoE$ ;
- $LCoE$  may be minimised by reducing the total number of WTs or the overall WF capacity, as well as maximising the WF-averaged values of  $D$  or  $\Omega$ , or minimising  $v_r$ ; increasing the WF-averaged values of  $P_r$  or  $H_{hub}$  is only beneficial for mid-potential sites;
- the mere maximisation of WF energy production is a misleading WFLO target, as corresponding to mid-to-high  $LCoE$  values; quite surprisingly, not particularly expensive WTs and energetically-efficient WF layouts are required to maximise  $AEY$ ;
- in contrast to various findings, the use of WTs with different  $P_r$ ,  $D$  or  $H_{hub}$  should be avoided in order to either minimising  $LCoE$  or maximising  $CF$ ; this finding has a relevant impact on WF layout design criteria, as only one combination for each WT provided by each manufacturer (i.e. the same WT installed throughout the WF) is recommended.

The study is affected by a number of limitations. The developed WFLO method has been applied for flat terrain, and so was the model used to assess the wake effects between the WTs (i.e. Jensen's model). Over complex terrain, conversely, a 1-D model such as Jensen's model is unable to fully describe the complex wake aspects as air flow turbulence that lead to increased fatigue load of WTs [61]. A WF of fixed size while varying the number of WTs was assumed, while the case with fixed number of WTs while varying WF size (as shown, e.g., by Chowdhury et al. [3]) was beyond the scope of the work. Theoretical wind conditions occurring across a "typical" atmospheric boundary layer were considered. Furthermore, a "reasonable" rather than genuinely "optimal" WT placement in the WF was assumed, as WT placement optimization was beyond the scopes of the study.

Future research directions might include application of current method to discrete grid-based layouts, attempting to improve the most prominent grid-based WFLO literature studies while considering the same assumptions and constraints as well as taking WT grid allocation as an input. In perspective, possible improvements of the proposed method, resulting from the need of overcoming some of current limitations, might deal with: (i) other types of sites, e.g. onshore sites with complex terrain, or offshore sites; (ii) more realistic wind conditions, representative of a greater variety of sites, or a systematic analysis of method's performances while varying wind conditions (as addressed, e.g., by Antonini et al. [62]); (iii) less limiting WF layout constraints, particularly those related to the shape and overall size (optimal WF size could be a further optimization function); (iv) a suitable combination of optimal WT type selection and optimal WT placement in the WF.

## Declaration of interest

The authors declare that they have no known competing financial interest.

## Acknowledgments

The WFLO problem addressed in this study is not a fragment of similar research carried out by the Author or other research group.

## Appendix A. Supplementary data

Supplementary data to this article can be found online at <https://doi.org/10.1016/j.enconman.2019.04.059>.

## References

- [1] Patel J, Savani V, Patel V, Patel R. Layout optimization of a wind farm to maximize the power output using enhanced teaching learning based optimization technique. *J Cleaner Prod* 2017;158:81–94.
- [2] Chen J, Wang F, Stelson KA. A mathematical approach to minimizing the cost of energy for large utility wind turbines. *Appl Energy* 2018;228:1413–22.
- [3] Chowdhury S, Zhang J, Messac A, Castillo L. Unrestricted wind farm layout optimization (UWFLO): investigating key factors influencing the maximum power generation. *Renew Energy* 2012;38(1):16–30.
- [4] Parada L, Herrera C, Flores P, Parada V. Assessing the energy benefit of using a wind turbine micro-siting model. *Renew Energy* 2018;118:591–601.
- [5] MirHassani SA, Yarahmadi A. Wind farm layout optimization under uncertainty. *Renew Energy* 2017;107:288–97.
- [6] Parada L, Herrera C, Flores P, Parada V. Wind farm layout optimization using a Gaussian-based wake model. *Renew Energy* 2017;107:531–41.
- [7] Gonçalves N, Sandou G, Siguereidjane H, Faillé D, Loevenbruck P. Wind farm distributed PSO-based control for constrained power generation maximization. *Renew Energy* 2019;133:103–17.
- [8] Serrano González J, Burgos Payán M, Riquelme Santos JM, González-Longatt F. A review and recent developments in the optimal wind-turbine micro-siting problem. *Renew Sustain Energy Rev* 2014;30:133–44.
- [9] Sun H, Yang H, Gao X. Investigation into spacing restriction and layout optimization of wind farm with multiple types of wind turbines. *Energy* 2019;168:637–50.
- [10] Pookpunt S, Ongsakul W. Design of optimal wind farm configuration using a binary particle swarm optimization at Huasai district, Southern Thailand. *Energy Convers Manage* 2016;108:160–80.
- [11] Feng J, Shen W, Li Y. An optimization framework for wind farm design in complex terrain. *Appl Sci* 2018;8(11):2053.
- [12] Eroğlu Y, Seçkiner SU. Design of wind farm layout using ant colony algorithm. *Renew Energy* 2012;44:53–62.
- [13] Castellani F, Buzzoni M, Astolfi D, D'Elia G, Dalpiaz G, Terzi L. Wind turbine loads induced by terrain and wakes: an experimental study through vibration analysis and computational fluid dynamics. *Energies* 2017;10(11):1839.
- [14] Karlina-Barber S, Mechler S, Nitschke M. The effect of wakes on the fatigue damage of wind turbine components over their entire lifetime using short-term load measurements. *J Phys Conf Ser* 2016;753(7):072022.
- [15] Yuan Y, Tang J. On advanced control methods toward power capture and load mitigation in wind turbines. *Engineering* 2017;3(4):494–503.
- [16] Mosetti G, Poloni C, Diviacco B. Optimization of wind turbine positioning in large wind farms by means of a genetic algorithm. *J Wind Eng Ind Aerodyn* 1994;51:105–16.
- [17] Jensen NO. A note on wind generator interaction. Risø-M-2411. Risø National Laboratory; 1983.
- [18] Ulku I, Alabas-Ulus C. A new mathematical programming approach to wind farm layout problem under multiple wake effects. *Renew Energy* 2019;136:1190–201.
- [19] Wu YT, Liao TL, Chen CK, Lin CY, Chen PW. Power output efficiency in large wind farms with different hub heights and configurations. *Renew Energy* 2019;132:941–9.
- [20] Chowdhury S, Zhang J, Messac A, Castillo L. Optimizing the arrangement and the selection of turbines for wind farms subject to varying wind conditions. *Renew Energy* 2013;52:273–82.
- [21] Abdulrahman M, Wood D. Investigating the power-COE trade-off for wind farm layout optimization considering commercial turbine selection and hub height variation. *Renew Energy* 2017;102:267–78.
- [22] Abdelsalam AM, El-Shorbagy MA. Optimization of wind turbines siting in a wind farm using genetic algorithm based local search. *Renew Energy* 2018;123:748–55.
- [23] Feng J, Shen WZ. Solving the wind farm layout optimization problem using random search algorithm. *Renew Energy* 2015;78:182–92.
- [24] Ali M, Matevosyan J, Milanović JV. Probabilistic assessment of wind farm annual energy production. *Electr Power Syst Res* 2012;89:70–9.
- [25] Wang L, Zhou Y, Xu J. Optimal irregular wind farm design for continuous placement of wind turbines with a two-dimensional Jensen-Gaussian wake model. *Appl Sci* 2018;8(12):2660.
- [26] Rahbari O, Vafaeipour M, Fazelpour F, Feidt M, Rosen MA. Towards realistic designs of wind farm layouts: application of a novel placement selector approach. *Energy Convers Manage* 2014;81:242–54.
- [27] Wang L, Tan AC, Cholette M, Gu Y. Comparison of the effectiveness of analytical wake models for wind farm with constant and variable hub heights. *Energy Convers Manage* 2016;124:189–202.
- [28] Katic I, Hostrup J, Jensen NO. A simple model for cluster efficiency. Proceedings of the European wind energy association conference and exhibition. 1986. p. 407–10.
- [29] Mortensen NG, Heathfield DN, Myllerup L, Landberg L, Rathman O. Wind atlas analysis and application program: WAsP 8 help facility. Roskilde, Denmark: Risø National Laboratory; 2005.
- [30] Nielsen P. The WindPRO manual edition 2.5. EMD International A/S; 2006.
- [31] González-Longatt F, Wall P, Terzija V. Wake effect in wind farm performance: steady-state and dynamic behavior. *Renew Energy* 2012;39:329–38.
- [32] Wang L, Tan AC, Gu Y. Comparative study on optimizing the wind farm layout using different design methods and cost models. *J Wind Eng Ind Aerodyn* 2015;146:1–10.
- [33] Rajper S, Amin IJ. Optimization of wind turbine micrositing: a comparative study. *Renew Sustain Energy Rev* 2012;16(8):5485–92.
- [34] Spera DA. Wind turbine technology: fundamental concepts of wind turbine engineering. 2nd ed. New York: ASME Press; 2009.
- [35] Pallabazzer R. Parametric analysis of wind siting efficiency. *J Wind Eng Ind Aerodyn* 2003;91(11):1329–52.
- [36] Gualtieri G. Improving investigation of wind turbine optimal site matching through the self-organizing maps. *Energy Convers Manage* 2017;143:295–311.
- [37] Wind turbines models. <https://en.wind-turbine-models.com>; 2019 [accessed 11/01/19].
- [38] International Renewable Energy Agency (IRENA). Renewable power generation costs in 2017. IRENA, ISBN 978-92-9260-040-2. Abu Dhabi, 2018. Available at: <https://www.irena.org/publications/2018/Jan/Renewable-power-generation-costs-in-2017> [accessed 11/01/19].
- [39] Chen Y, Li H, Jin K, Song Q. Wind farm layout optimization using genetic algorithm with different hub height wind turbines. *Energy Convers Manage* 2013;70:56–65.
- [40] Fingersh LJ, Hand MM, Laxson AS. Wind turbine design cost and scaling model. Golden, CO: NREL Report No. TP-500-40566; 2006.
- [41] Kohonen T. Self-organizing maps. 2nd ed. Heidelberg, Germany: Springer; 2001.
- [42] Beccali M, Cirrincione G, Marvuglia A, Serpota C. Estimation of wind velocity over a complex terrain using the generalized mapping regressor. *Appl Energy* 2010;87(3):884–93.
- [43] Wenyi L, Zhenfeng W, Jiguang H, Guangfeng W. Wind turbine fault diagnosis method based on diagonal spectrum and clustering binary tree SVM. *Renew Energy* 2013;50:1–6.
- [44] National Renewable Energy Laboratory (NREL). Wind resource assessment handbook. Golden, CO: NREL report no. TAT-5-15283-01, April 1997. Available: <https://www.nrel.gov/docs/legosti/fy97/22223.pdf> [accessed 11/01/19].
- [45] Gualtieri G. A comprehensive review on wind resource extrapolation models applied in wind energy. *Renew Sustain Energy Rev* 2019;102:215–33.
- [46] Gualtieri G. Atmospheric stability varying wind shear coefficients to improve wind resource extrapolation: a temporal analysis. *Renew Energy* 2016;87:376–90.
- [47] Bañuelos-Ruedas F, Angeles-Camacho C, Ríos-Marciello S. Analysis and validation of the methodology used in the extrapolation of wind speed data at different heights. *Renew Sustain Energy Rev* 2010;14(8):2383–91.
- [48] Gualtieri G. Development and application of an integrated wind resource assessment tool for wind farm planning. *Int J Renew Energy Res* 2012;2(4):674–85.
- [49] WindPower. The wind turbines and wind farms database. 2019 [accessed 11/01/19]. <http://www.thewindpower.net>.
- [50] Moné C, Smith A, Maples B, Hand M. 2013 Cost of wind energy review. Golden, CO: NREL Report No. TP- 5000-63267; 2015.
- [51] Boudia SM, Guerri O. Investigation of wind power potential at Oran, northwest of Algeria. *Energy Convers Manage* 2015;105:81–92.
- [52] Stevens RJ, Hobbs BF, Ramos A, Meneveau C. Combining economic and fluid dynamic models to determine the optimal spacing in very large wind farms. *Wind Energy* 2017;20(3):465–77.
- [53] Patel MR. Wind and solar power systems: design, analysis, and operation. Boca Raton, FL: Taylor & Francis; 2006.
- [54] Masters GM. Renewable and efficient electric power systems. Hoboken, New Jersey: John Wiley & Sons; 2004.
- [55] Lissaman P, Zaday A, Gyatt G. Critical issues in the design and assessment of wind turbine arrays. Proc. 4th international symposium on wind energy systems, Stockholm. 1982.
- [56] Meyers J, Meneveau C. Optimal turbine spacing in fully developed wind farm boundary layers. *Wind Energy* 2012;15:305–17.
- [57] Mirghaed MR, Roshandel R. Site specific optimization of wind turbines energy cost: iterative approach. *Energy Convers Manage* 2013;73:167–75.
- [58] Bowman AW, Azzalini A. Applied smoothing techniques for data analysis: the Kernel approach with S-plus illustrations. Oxford: Oxford University Press; 1997.
- [59] Bowman AW. 'sm' package: smoothing methods for nonparametric regression and density estimation. Version 2.2-5.6, 2018/09/27. Available at: <https://cran.r-project.org/web/packages/sm/index.html> [accessed 11/01/19].
- [60] Vasel-Be-Hagh A, Archer CL. Wind farm hub height optimization. *Appl Energy* 2017;195:905–21.
- [61] Wang L, Cholette ME, Zhou Y, Yuan J, Tan AC, Gu Y. Effectiveness of optimized control strategy and different hub height turbines on a real wind farm optimization. *Renew Energy* 2018;126:819–29.
- [62] Antonini EG, Romero DA, Amon CH. Continuous adjoint formulation for wind farm layout optimization: a 2D implementation. *Appl Energy* 2018;228:2333–45.